

Understanding the Nuclear Gas Dispersion in Early-Type Galaxies in the Context of Black Hole Demographics¹

Gijs A. Verdoes Kleijn,^{2,3} Roeland P. van der Marel,⁴ Jacob Noel-Storr^{4,5}

ABSTRACT

The majority of nearby early-type galaxies contains detectable amounts of emission-line gas at their centers. The nuclear gas kinematics form a valuable diagnostic of the central black hole (BH) mass. Here we analyze and model HST/STIS observations of a sample of 27 galaxies; 16 Fanaro & Riley Type I radio galaxies and 11 (more) normal early-type galaxies. We focus here on what can be learned from the nuclear velocity dispersion (line width) of the gas as a complement to the many studies dealing with gas rotation velocities. We find that the dispersion in a STIS aperture of 0.1^{00} – 0.2^{00} generally exceeds the large-scale stellar velocity dispersion of the galaxy. This is qualitatively consistent with the presence of central BHs, but raises the questions whether the excess gas dispersion is of gravitational or non-gravitational origin and whether the implied BH masses are consistent with our current understanding of BH demography (as predicted by the M – σ relation between BH mass and stellar velocity dispersion). To address this we construct purely gravitational axisymmetric dynamical models for the gas, both thin disk models and models with more general axis ratios and velocity anisotropies. For the normal galaxies the nuclear gas dispersions are adequately reproduced assuming disks around BHs with masses that follow the M – σ relation. In contrast, the gas dispersions observed for the radio galaxies generally exceed those predicted by any of the models. We attribute this to the presence of non-gravitational motions in the gas that are similar to or larger than the gravitational motions. The non-gravitational motions are presumably driven by the active galactic nucleus (AGN), but we do not find a relation between the radiative output of the AGN and the non-gravitational dispersion. Given the uncertainties about the dynamical state of the gas,

¹Based on observations with the NASA/ESA Hubble Space Telescope obtained at the Space Telescope Science Institute, which is operated by the Association of Universities for Research in Astronomy, Incorporated, under NASA contract NAS5-26555.

²ESO, Karl-Schwarzschild-Strasse 2, 85748, Garching bei Muenchen, Germany

³current address: Kapteyn Astronomical Institute, Groningen, 9700 AV, The Netherlands

⁴Space Telescope Science Institute, 3700 San Martin Drive, Baltimore, MD 21218.

⁵current address: Steward Observatory, University of Arizona, 933 N Cherry Ave., Tucson, AZ 85721

it is not possible to uniquely determine the BH mass for each galaxy from its nuclear gas dispersion. However, for the sample as a whole the observed dispersions do not provide evidence for significant deviations from the $M_{\text{BH}} - \sigma$ relation.

Subject headings: galaxies: elliptical and lenticular, cD | galaxies: nuclei | galaxies: kinematics and dynamics | galaxies: active | ISM : kinematics and dynamics.

1. Introduction

The mass of a central black hole (BH) in a galaxy can be directly weighed using gravitational ‘test particles’ moving around it (see e.g., Komberg & Richstone 1995). Commonly used test particles are stars, optical emission-line gas and maser clouds. These move around in the combined potential well of the stellar mass and the central black hole mass. A secure direct dynamical measurement of the BH mass requires that the distribution and kinematics of the test particles are measured in the immediate vicinity of the BH, i.e., the ‘black hole’s sphere of influence’, so that its gravitational potential has a measurable effect on the kinematics in addition to the effect of the stellar mass potential. Ground-based optical telescopes can resolve the BH’s sphere of influence only for very nearby galaxies, with our Milky Way being a spectacular nearby example (e.g., Ghez et al. 2003; Schodel et al. 2003). The Hubble Space Telescope (HST) can provide the required spatial resolution for galaxies with distances up to several tens of Mpc (e.g., Komberg & Gebhardt 2001). The Very Long Baseline Interferometer (VLBI) can in principle probe BH masses out to even larger distances provided that the galaxies display nuclear maser emission. Together these methods have led to direct dynamical measurements of BH masses M_{BH} in the range $M_{\odot} \approx 10^6 - 10^9 M_{\odot}$ in several tens of galaxies in the nearby Universe (see e.g., Tremaine et al. 2002; Marconi et al. 2003 for listings of BH mass measurements). The BH masses are mostly based on dynamical modeling of kinematics of either stars or emission-line gas. The detected black hole masses M_{BH} correlate well with both host spheroidal luminosity L_B , global stellar velocity dispersion σ_s and spheroidal mass (Gebhardt et al., 2000; Ferrarese & Merritt, 2000; Tremaine et al. 2002; Marconi et al. 2003; Haring & Rix 2004). These correlations roughly represent our current knowledge of the local BH demography. To explore these correlations further, i.e., their scatter and extent in BH mass, dynamical modeling using emission-line gas kinematics in early-type galaxies is convenient and in some respects even crucial. First of all, more than 50% of the early-type galaxies in the nearby Universe contain gas at their centers (e.g., Goudfrooij et al. 1994; Ho, Filippenko & Sargent 1997). Second of all, the most massive black holes currently found (i.e., $M_{\text{BH}} \approx 10^6 - 10^9 M_{\odot}$) are often in giant ellipticals. The central stellar surface brightness of these galaxies is typically too low to obtain accurate stellar kinematics with HST and maser emission has not been detected (e.g., Barth et al. 2004).

At the centers of galaxies, the collisional gas is expected to settle quickly into a disk, if unperturbed by forces other than gravity (e.g., Habe & Ikeuchi 1985). The frequent detection with HST of disk-like structures in dust and gas in early-type galaxies suggests that settling actually takes place (e.g., van Dokkum & Franx 1995; Tran et al. 2001; Verdoes Kleijn et al. 1999; Laine et al. 2003). Therefore the extended gas velocities in galactic nuclei have been modeled assuming a thin disk in circular rotation. Such models have been successful in explaining the observed gas

velocities. However, in the few cases where both gas velocities and gas dispersions are modeled, it is often found that the nuclear velocity dispersion exceeds the prediction for a thin disk (van der Marel & van den Bosch 1998; Barth et al. 2001; Maciejewski & Binney 2001; Cappellari et al. 2002; Verdoes Kleijn et al. 2002). Many of these targets are AGN and display regular disks of dust and gas. The origin of this ‘excess’ velocity dispersion is unknown. Two common ad-hoc assumptions are that: (a) the excess dispersion is due to non-gravitational ‘turbulent’ forces of unknown origin which do not affect the mean circular rotation of the gas (e.g., van der Marel & van den Bosch 1998; Verdoes Kleijn et al. 2002); or (b) the excess dispersion is purely gravitational and affects the rotation of the gas through the asymmetric drift equation (e.g., Barth et al. 2001).

A main aim of this paper is to determine which early-type galaxies do and which do not display an excess in nuclear gas dispersion. If there are galaxies for which the disk remains thin all the way to the nucleus, then any velocity dispersion observed through a nuclear aperture is caused by differential rotation over this aperture. A nuclear aperture samples gas which is much closer to the BH than a series of apertures which samples the extended rotation curve. Hence, the nuclear gas dispersion can be sensitive to much lower black hole masses than the rotation curve. This is relevant as the sensitivity in terms of the minimum detectable BH mass in early-type galaxies with stellar dynamical methods or with gas rotation velocities is typically not much below the values predicted by the correlations between BH mass and spheroid properties. A relevant example in this case is the claim that active spiral galaxies classified as Narrow Line Seyfert 1s harbor BHs with masses smaller than those predicted by the $M_{\text{BH}} - M_{\text{bulge}}$ relation (e.g., Grupe & Mathur 2004).

For the galaxies with nuclear gas dispersions in excess of that expected from a thin disk, we want to determine the origin of this excess. On the one hand, if it has a gravitational origin, this implies that the gas should rotate less fast than the circular speed and the thin-disk approximation does not hold. The gas might then have a distribution somewhere in the range from a thin disk to a purely spherical distribution. Previous BH mass estimates based on the assumption of thin disks would then be underestimated, and this would affect the observed correlations between black hole mass and large-scale spheroid properties. On the other hand, if the excess dispersion has a non-gravitational origin, we would like to quantify how it depends on galaxy parameters, such as nuclear activity. This in turn could shed light on the accretion process in these nearby, typically low-luminosity, AGN.

In summary, this paper studies the nature of the line widths of emission-gas in nearby early-type galaxy nuclei and its implications for the BH demography and BH accretion processes. A similar study into the line-widths of gas for late-type galaxies has been performed by Sarzi et al. (2002). The outline of the paper is as follows. Section 2 describes the sample selection, the data and the determination of the central gas velocity dispersions. Section 3 compares the observed dispersions to those expected from a thin circular disk. Section 4 compares the observed dispersions to those expected from a gas distribution which is more spheroidal than a disk. Section 5 constrains the direction of the non-gravitational dispersion. Section 6 describes the caveats of our modeling. Finally, Section 7 provides a discussion of the results and lists the main conclusions of the paper. Throughout the paper we use a Hubble constant $H_0 = 75 \text{ km s}^{-1} \text{ Mpc}^{-1}$.

2. Sample and Data Analysis

We analyze a sample of 27 galaxies. It consists of galaxies which meet the following requirements: (a) early-type host morphology; (b) distance below 110 Mpc; (c) a large-scale stellar velocity dispersion measurement is available from the literature; (d) HST imaging exists that shows an identifiable (i.e., relatively unobscured) nucleus; (e) HST emission line spectroscopy exists for which kinematics and flux profiles were published (20 galaxies) or which are available in the HST archive (7 galaxies). We excluded galaxies for which the signal-to-noise ratio of the spectrum was very low, complicating a reliable analysis. Sixteen of the galaxies are classified as Fanaro & Riley Type I radio galaxies with jets on scales of tens of kpc or larger. The other 11 galaxies also have radio emission. Their radio luminosity is typically much lower (cf. Table 1) and the radio emission originates from a central compact component. We reduced and analyzed the archival data for the 7 galaxies similarly as in our previous papers (e.g., Noel-Storr et al. 2003; Verdoes Kleijn et al. 2002). The spectra for all galaxies except two were obtained with HST/STIS in combination with the G750M grating. For IC 1459 a HST/STIS spectrum with the G430L grating was obtained and for NGC 6251 a HST/FOS spectrum with the $0.1''$ PAIRB aperture. All spectra cover the H + [N II] and [S II]6716,6731 lines, except for the G430L spectrum of IC 1459. In that case we use the H line for our analysis. Table 1 lists basic data for the sample galaxies.

The first step is to determine the gas velocity dispersions in the central region of each galaxy. In most cases (both in the literature and in our analysis of the archival spectra) single Gaussians were fitted to each of the lines of the H + [N II] composite and to the weaker [S II]6716, 6731 lines. Only in NGC 3245 and NGC 4526 are the [S II] lines too weak to be fitted. For NGC 6251 we used the fit to the H + [N II] lines available in Ferrarese & Ford (1999). For these narrow components, the [N II] 6584 was the strongest line in 85% of the galaxies. In four galaxies (NGC 3245, NGC 3998, NGC 4278 and NGC 6251) a broad emission-line component is clearly present in addition to the narrow H + [N II] components. This is most likely due to a broad H component because the broad component is not seen in the [S II] forbidden lines and the forbidden [N II] lines originate presumably in the same region as the [S II] lines. This broad component was fitted with an additional Gaussian. For the two archival sources with a broad component (NGC 3998 and NGC 4278) we established that the [S II] lines provide an important fitting constraint in addition to the H + [N II] region which is blended heavily due to the broad component. Excluding the [S II] doublet from the fit results in 35% larger (NGC 3998) or smaller (NGC 4278) dispersion. Similarly, Ferrarese & Ford (1999) report for NGC 6251 a width of the [S II] lines which is 37% larger than the H + [N II] lines at the nuclear aperture. For the archival cases with only narrow lines, we determined that the inferred gas dispersion changes by $\sim 10\%$ by excluding the [S II] doublet from the fit.

The next step is to find for each galaxy the aperture closest to the nucleus which we will refer to as the 'central' aperture. We assume that the dynamical nucleus coincides with the peak in emission-line and continuum flux. The typical dimension of the STIS apertures is $0.1'' \times 0.2''$ in the spectral direction and $0.05'' \times 0.1''$ in the spatial direction (see Table 2). The exact sub-pixel location along the slit of the nucleus was determined by fitting a Gaussian to the central few emission-line fluxes. In most cases the peak in velocity dispersion coincides with the flux peak. We indicate in Table 1 the few cases in which the maximum dispersion does not peak at the central aperture but

just outside it. The exact location of the nucleus (i.e., the flux peak under our assumptions) in the direction of the slit width is not known. We assume that it is centrally located in this direction. This seems plausible given that the target acquisition procedure is designed to have the center of the slit located exactly on the brightest continuum point in the galaxy. That this ‘peak-up’ procedure actually succeeded is supported by the steep decline in flux in parallel slits which are available for many targets. Nevertheless, the effect on our results of a potential offset from this location is discussed in Section 6. The gas velocity dispersion σ_g at the central aperture is listed in Table 1. The typical relative formal measurement error for σ_g is 5%.

We also require the unconvolved flux profile for our analysis. The emission-line surface brightness is represented by fitting a double exponential function,

$$I(R) = I_1 \exp(-R/R_1) + I_2 \exp(-R/R_2); \quad (1)$$

to the narrow emission-line fluxes taking into account the PSF and disk inclination (see e.g., Verdoes Kleijn et al. 2002 for a detailed description). The disk inclinations were taken from the literature or determined by us from the extended dust disk often present on HST imaging. If dust is absent or the inclination could not be determined reliably, we assumed $i = 60^\circ$. The HST observational characteristics, unconvolved flux profiles and disk inclinations are listed in Table 2. The fluxes are typically fitted within the formal errors or within 10%. A few galaxies have some asymmetry in their profiles over which the symmetric averages, namely IC 1459, NGC 3245, NGC 4278, NGC 4459 and NGC 4486.

Finally, we use published stellar dispersions (see Table 1). The stellar dispersions σ_s are measured through an aperture of typically several arcsec². This corresponds to a region much larger than the BH sphere of influence, and measures primarily the virial dispersion of the system as a whole. We will make use of the stellar dispersions to estimate black hole masses using the M - σ_s relation as determined by Tremaine et al. (2002). The relation is calibrated to flux-weighted stellar dispersions σ_e inside an effective radius of the galaxy, which are not available for most of our sample galaxies. However, comparing σ_e and σ_s where possible shows a difference of typically 7% between σ_s and σ_e . We will use this as the typical relative error on our measurement of σ_s in approximation to σ_e . Lastly, Table 1 also lists the black hole masses obtained from dynamical modeling of central gas disk rotation velocities as published for eight galaxies in the sample.

3. Thin Disk Models

Figure 1 shows the central gas velocity dispersion at small scales (i.e., typical aperture size $0.15''$ or 40 pc for typical galaxy distance of 50 Mpc) versus the large-scale stellar dispersions (tracing the flux-weighted dispersion at kpc scales). The nuclear gas dispersions are almost always larger than the large-scale stellar dispersions, increasingly so for larger stellar dispersions. Given the success rate of black hole mass determinations in early-type galaxies, it now seems quite possible that all spheroids harbor a black hole at their nucleus. There are two generic ways in which the presence of a BH can contribute to the nuclear gas dispersion. First, gas motions increase at smaller distances from a central black hole due to the increase of the gravitational force. Integrated over a

nite aperture this will lead to a larger observed gas dispersion. We will call this the gravitational contribution. An increase will occur always, but its magnitude will depend on the physical structure and orbital distribution of the gas, e.g., a thin rotating disk or a more spheroidal distribution. The effect is noticeable because for a typical $\sigma_s = 250 \text{ km s}^{-1}$ in our sample, the typical central HST aperture is only a factor two larger than the rough measure of the black hole radius of influence $r_{\text{BH}} = GM_s^{-1/2} \approx 20 \text{ pc}$ adopting the M_s relation from Tremaine et al. (2002). The relation finds M_s with σ_s^4 . If the gas motions are dominated by gravitation it is expected that M_s with σ_s^2 and hence $\sigma_g \propto \sigma_s^2$ qualitatively consistent with the increasing ratio of σ_g and σ_s shown in Figure 1. The M_s relation also suggests that one should expect a smaller excess gas dispersion in galaxies with smaller σ_s for another reason: galaxies with smaller σ_s have a smaller BH mass and a sphere of influence so that a STIS aperture of fixed size samples more of the gas outside of the BH sphere of influence. A second generic way in which the presence of a BH can contribute to the nuclear gas dispersion is not through its gravitational force, but through input of kinetic energy which perturbs the collisional gas. We will call this the hydrodynamical or non-gravitational contribution. This energy could be released by processes related to an active black hole. As a side remark, it is unlikely that the kinetic energy might be provided by collisions with photons emerging from the active region around the black hole. The reason is that the bolometric luminosity of the low-luminosity active nuclei discussed here is always orders of magnitudes below the Eddington luminosity (e.g., Ho 1999). Shocks, e.g., jet-gas interactions are a more plausible source of kinetic energy. It could be that the gravitational contribution dominates (e.g., a thin disk of non-colliding gas particles in circular rotation) or that the hydrodynamical contribution dominates (e.g., a fully collisionally driven outflow of gas from the active black hole). The well-defined thin dust and gas disks often seen immediately outside the nucleus in these galaxies suggest that the gas might be settled all the way to the nucleus. Therefore, we will first determine the answer to the question: in which galaxies can the BH potential account for the observed nuclear gas dispersion assuming that the gas is located in a thin circular disk?

The answer to this question is known already for five galaxies in our sample for which detailed modeling has been performed of both gas velocities and dispersions of the extended gas disk under the assumption of a thin circular disk. In the case of NGC 7052 (van der Marel & van den Bosch 1998), IC 1459 (Cappellari et al. 2002; Verdoes Kleijn et al. 1999) and NGC 4335 (Verdoes Kleijn et al. 2002), an excess of dispersion by a factor 2 or more was observed. For NGC 3245 (Barth et al. 2001), a smaller excess of 35% was observed. In the case of M 87 (Machetto et al. 1997; Hamers et al. 1994), no dispersion excess was observed. The velocity dispersion for this galaxy was accounted for by a model in which the gas resides in an annulus instead of a disk. (This model can also account well for the velocities and peculiarities in the flux distribution.) It is these mixed results on excess gas dispersion that lead us to examine the presence of excess gas dispersion for a larger sample of galaxies.

In the present and following sections (Section 3-5) we present results of dynamical models of the gas velocity dispersions. Caveats that result from the assumptions in our models are discussed in Section 6. Performing gas disk kinematical modeling for our complete sample in similar detail as done for the aforementioned few cases is beyond the scope of this paper. Thus we constructed somewhat more simplified thin disk models. The main simplification is to neglect the stellar mass

contribution to the central gravitational potential. The effect of this simplification on the predicted velocity dispersions for the galaxy sample can be estimated as follows. Assume a spherical stellar mass density $\rho(r) = \rho_0 (r=r_0)$ in the nuclear region, where r is the radius in pc and ρ_0 a scaling constant. According to the LEDA database, the absolute blue magnitude in our sample varies in the range $M_B = [19.3; 22.5]$ with a mean $\langle M_B \rangle = 21.1$. Assuming a typical galaxy color $B - V = 0.95$, this indicates that a typical galaxy in our sample is about 1 magnitude brighter than the division magnitude at $M_V = 21.0$ between shallow core and steep core ("power-law") galaxies (Gebhardt et al. 1996). Galaxies brighter than this division magnitude typically have $\rho_0 = 1$ (while below they have $\rho_0 = 2$). From the study by Gebhardt et al. (1996) we infer a typical $\rho_0 = 10^4 M_\odot \text{pc}^{-3}$. With this information we can compute the circular velocity $v_{c,s}$ due to the stellar mass at a given radius as $v_{c,s}^2 = 4 G \rho_0 \frac{r^2}{r+3}$. By comparison, the circular velocity due to the BH is $v_{c,BH}^2 = \frac{GM}{r}$. We compute the ratio of these two at $r = 0.1^{00}$ from the nucleus assuming a BH mass according to the M relation. The value $r = 0.1^{00}$ is a typical distance from the galaxy center at which we have measured gas dispersions with HST. The ratio of the circular velocities in quadrature (i.e., equivalent to the ratio in dynamical mass) is always less than 20%. This is much smaller than, e.g., the scatter of 0.3 dex in the M relation (Tremaine et al. 2002). This confirms that the stellar mass contribution in our analysis can be safely neglected, provided that: (a) the BH masses are not significantly below the M relation; and (b) we are not attempting to model the large scale rotation of the gas at radii much beyond 0.1^{00} . As an additional check we directly determined the difference in predicted dispersion with and without BH mass for NGC 4335, NGC 7052 and IC 1459. For these galaxies, we modeled the stellar mass in previous papers (Verdoes Kleijn et al. 2002; van der Marel & van den Bosch 1998; Verdoes Kleijn et al. 1999). These cases confirm the result from the general argument that the difference in predicted dynamical masses is always less than 20% (see also Figure 2, discussed below).

For a thin circular disk, the velocity dispersion observed in a nuclear aperture is due entirely to differential rotation over the aperture. To calculate this dispersion we used the modeling software that is described in more detail in van der Marel & van den Bosch (1998) and Verdoes Kleijn et al. (2000; 2002). This modeling takes into account the emission-line flux profile, slit width and PSF convolution. We first modeled the galaxies for which a BH mass estimate is available in the literature from detailed modeling of the gas rotation velocities. Figure 2 shows the predicted versus observed velocity dispersions for these eight galaxies. Seven galaxies have an observed dispersion in excess of the prediction. The modeling nicely reproduces the aforementioned relative differences in excess dispersion for M 87, NGC 3245, NGC 7052, NGC 4335 and IC 1459 known from prior modeling of the rotation velocities in the extended gas disk. To put the complete sample in a similar diagram, we need an estimate of the BH mass for every galaxy. For this we use the M relation as calibrated by Tremaine et al. (2002). They derive the relation $\log[M(M_\odot)] = 8.13 + 4.02 \log(\sigma = 200 \text{ km s}^{-1})$. The slope of this relation falls between those reported by Gebhardt et al. (2000; slope= 3.75) and Ferrarese & Merritt (2000; slope= 5.27). Figure 3 shows the predicted versus observed dispersion for a thin disk model, but now assuming for all galaxies a BH mass according to the M relation. The observed dispersions in non-radio galaxies scatter around the prediction from the model (except for IC 989: cf. Section 7). In fact, the number of non-radio galaxies and their range in observed gas dispersions is large enough that they independently confirm the M relation for the thin

disk model. This is non-trivial because BH masses significantly below the $M_{\text{BH}} - \sigma$ relation could have been detected with the HST/STIS observations. As a measure of the minimally detectable BH mass, we compute the BH mass which causes a gas dispersion which equals that predicted from the combined effect of instrumental broadening and the stellar mass model discussed above. We use again the typical radius of 0.1^{10} and take into account the disk inclination and distance for each galaxy. The resulting masses vary between $6 \times 10^6 M_{\odot}$ and $6 \times 10^7 M_{\odot}$ with a typical value of $3 \times 10^7 M_{\odot}$. (Exceptions are NGC 3862 and UGC 7115. Their minimally detectable BH mass lies above the $M_{\text{BH}} - \sigma$ relation because the instrumental line broadening is larger than the dispersion due to differential gravitational rotation for such close to face-on gas disks.) The BH masses predicted by the $M_{\text{BH}} - \sigma$ relation exceed this typical detectable BH mass by a factor 2 for the lowest stellar dispersions and by almost 2 orders of magnitude for the highest stellar dispersions in the sample. In conclusion, the gas dispersions in non-radio galaxies support the idea that all early-type galaxies harbor supermassive black holes at their nuclei with masses according to the $M_{\text{BH}} - \sigma$ relation.

In contrast to the non-radio galaxies, all radio galaxies have a gas dispersion in excess of that expected from the thin disk models. About 50% of those fall above the 1σ scatter expected from the intrinsic scatter in the $M_{\text{BH}} - \sigma$ relation. To explore the origin of this we plot in Figure 4 the ratio R_{ord} of observed dispersion and that predicted for the disk model. There is a trend of an increasing ratio with decreasing disk inclination. In fact, the four largest ratios are all in galaxies with gas disk inclinations $i < 40^\circ$, i.e., close to face-on disks. This cannot be explained as a result of measurement errors in the dust disk inclinations. The arrows in Figure 4 show by how much R_{ord} can decrease due to the known measurement errors. The decreases do not change the overall result that radio galaxies systematically have excess dispersions. A more extreme (and probably unphysical) possibility is to assume that we might have used incorrect inclinations because the measured dust disk inclinations bear no relation to the actual inner gas disk inclinations. However, this would still not provide a satisfactory explanation. If all the gas disks were in reality edge-on and well described by thin disk models, then we would have expected the points in Figure 4 to fall along the curve $R_{\text{ord}} = \sin^{-1} i$ (solid curve). This still falls below many of the observed dispersion ratios (see Figure 4). Moreover, an excess gas dispersion is not only seen in radio galaxies with relatively face-on disks. If we exclude systems with disk inclinations $i < 40^\circ$ from the analysis, the median $R_{\text{ord}} = 1.32$ for radio galaxies versus 0.96 for non-radio galaxies. A median test yields a probability of only 0.05 that this difference would occur by chance in the event that the samples were drawn from populations with the same median. Therefore, a solution to account for the excess gas dispersion in radio galaxies must probably be sought in having a significant vertical velocity dispersion component.

Finally, as a sanity check we analyzed the dependence of the R_{ord} on BH mass and the typical circular velocity of the system, parameterized as $\sqrt{\frac{GM}{r_{\text{HALF}}}}$ where r_{HALF} is the radius inside which half of the light of the unconvolved emission-line flux distribution is contained. There is no relation between the dispersion ratio and the two measures of the gravitational potential. This confirms that the excess velocity dispersion in the radio galaxies is not somehow an artifact of our gravitational modeling.

4. Spheroidal Models

Many galaxies in the sample show disks of dust and gas with radii ranging from hundreds of pc up to several kpc. It appears reasonable, but might be wrong to assume by extrapolation that the nuclear region within the spatial resolution of the observations also has a disk-like geometry. Instead, the gas distribution might be more spheroidal in the vicinity of the black hole. In that case the gas moves also out of the plane of the larger scale thin gas disk. This could explain qualitatively the observed increasing ratio of observed versus predicted dispersion for decreasing dust disk inclination. We address next whether such a spheroidal distribution can also quantitatively explain the observed σ_g gravitationally.

Gas in a vertically extended distribution (e.g., a spherical one) tends to collapse quickly to a disk due to hydrodynamical forces. Thus, to maintain a spheroidal structure, one would have to assume that the gas is located in individual clouds that move collisionlessly. As an initial assessment of the plausibility of this we estimate the collision time-scale for clouds in a simplistic model: spherical cloudlets of ionized hydrogen moving around in a spherical volume. The typical time t_{free} between cloudlet collisions is estimated as:

$$t_{\text{free}} = \frac{V}{N_{\text{cl}} \sigma_{\text{cl}} v_{\text{cl}}}; \quad (2)$$

where v_{cl} is the typical relative velocity of cloudlets, V is the spherical volume within which the cloudlets are contained, σ_{cl} is the cross-section of each cloudlet and N_{cl} is the total number of clouds. For V we take the spherical volume with a radius equal to the half-light radius of the gas distribution as seen projected on the sky. For v_{cl} we take the circular velocity at half the half-light radius. The number of cloudlets N_{cl} is computed from

$$N_{\text{cl}} = N = \left(\frac{4}{3} R_{\text{cl}}^3 n_e\right); \quad (3)$$

where N is the total number of electrons, n_e is the electron density and R_{cl} is the radius of each cloudlet. The electron density can be obtained from the relation between the flux ratio $[\text{II}] 6716 / 6731$ and the electron density (Osterbrock 1989). This flux ratio is only sensitive to electron densities in the range $[10^2; 10^4] \text{ cm}^{-3}$. Outside this range the flux ratio becomes constant as a function of n_e . We obtain the flux ratio for 15 of the radio galaxies from Noel-Storr et al. (2003) of which six lead to upper and lower limits on the electron density. N can be estimated as discussed in Osterbrock (1989) assuming case B recombination:

$$N = \frac{L_{\text{H}}}{n_e^{\text{eff}} h_{\text{H}}}; \quad (4)$$

where $h_{\text{H}}^{\text{eff}} = 3.03 \cdot 10^{14} \text{ cm}^{-3}$ is the recombination coefficient (assuming $T = 10^4 \text{ K}$) and h_{H} and L_{H} are the frequency and luminosity for $\text{H}\beta$. We obtain L_{H} from the central $\text{H}\beta + [\text{N II}]$ luminosity (Verdoes Kleijn et al. 2002) using the standard $L_{\text{H}\beta} = L_{\text{H}}$ ratio of 3.1 and the $[\text{N II}] 6548, 6584 / \text{H}\beta$ flux ratio determined from our Gaussian line fits. This results in the following equation for the collision time:

$$t_{\text{free}} = \frac{R_{\text{cl}}^{3.5} n_e^2}{M L_{\text{H}}}; \quad (5)$$

This increases linearly with the radius of the cloudlets R_{cl} . If we assume that R_{cl} is as large as a tenth of the half-light radius, then the inferred t_{free} varies between 10^3 yr and 10^{13} yr with a typical value of 10^7 yr. Some of the huge scatter is most likely due to the simplicity of the estimate. But either way, it appears unlikely that the gas could remain in a collisionless state for a significant fraction of the Hubble time. Collisions lead to dissipation, loss of energy, and settling onto circular orbits. However, this is only true if there is no energy input into the gas. That may well be incorrect for most of the galaxies in our sample, given that 16 galaxies are FR I radio galaxies, and the remainder have nuclear radio emission. If there is energy input, then the gas can maintain an extended distribution for much longer than the timescale t_{free} calculated above. Even though collisions would occur, one might expect the system to evolve through a sequence of states that are all approximately collisionless. Therefore, it is reasonable to study the predictions of collisionless models for the nuclear gas in our sample galaxies.

A major uncertainty in the calculation of collisionless models is the phase-space distribution of the clouds, which is needed to compute the observed velocity dispersion along the line of sight. The phase-space distribution involves a spatial component such as a radial number density profile. We do not know this profile. We only know the flux distribution, which could be quite different. The phase-space distribution also requires knowledge about the nature of the cloud kinematics, for example anisotropies in the velocity dispersion. These are also unknown. We therefore decided to explore the line-of-sight velocity dispersion for a plausible range of phase-space distributions. We use axisymmetric dynamical models presented in de Brujne et al. (1996). We explore gas clouds with an axisymmetric power-law number density distribution with axis ratio q (i.e., $(R; z) = (R^2 + z^2 = q^2)^{-(\alpha+2)}$) in the Kepler potential caused by the black hole. The gas clouds are assumed to have a constant velocity dispersion anisotropy $\beta = 1 - (\overline{v^2} + \overline{v_z^2}) / (2\overline{v_r^2})$ (i.e., the 'case II' models in de Brujne et al. 1996; cf. Binney 1980, with $(r; \theta; \phi)$ the usual spherical coordinates). Thus we have four free parameters: the number density scaling constant ρ_0 , the axis ratio q , the power-law slope α of the particle density profile and the velocity dispersion anisotropy β . These models require $\beta > 1 - 2 + \alpha$ to be physical. De Brujne et al. (1995) evaluated the projected velocity dispersions. The software to calculate them numerically is available from <http://www.stsci.edu/~marel/>.

We want to know how different the observed velocity dispersion for a spheroid can be compared to the dispersion for a thin disk, for a plausible range of the free parameters. Thus we determined the ratio R_{sxd} of the velocity dispersions for a spheroid and a thin disk that have the same projected surface density distribution and apparent axial ratio. The latter criterion fixes the ratio of the ρ_0 values for the two models, and implies that R_{sxd} is independent of ρ_0 . We define R_{sxd} as the ratio of the line-of-sight dispersion weighted by the number density and integrated over an aperture which is typical for the observations. The result depends on power-law slope, axis ratio and dispersion anisotropy. We explored the parameter ranges $\alpha = [1.5; 10]$, $q = [0.1; 0.9]$ and $\beta = [-\infty; 1]$, which should encompass all plausible models. Figure 5 shows R_{sxd} as a function of apparent axis ratio for the quoted parameter ranges. Regardless of the choice of parameters, the modeled spheroidal distributions have increased velocity dispersions in comparison to thin disks only for $q < 0.7$ (corresponding to inclinations $i < 45^\circ$ for a thin disk).

As also shown in Figure 4, the non-radio galaxies scatter around $R_{o,d} = 1$ indicating that their dispersions are consistent with thin disks in circular rotation around BHs that follow the M

relation. By contrast, the radio galaxies have dispersion ratios $R_{o,d}$ which are systematically larger than 1, and also larger than the $R_{s,d}$ expected for collisionless spheroidal models. So it seems unlikely that a spheroidal distribution of collisionless gas clouds can account for the nuclear gas velocity dispersions in radio galaxies. We also explored the ratio of the velocity dispersions for an axisymmetric spheroid and a disk at the same inclination instead of the same apparent axis ratio¹. The reason is that the axis ratio of the gas distribution at the nucleus is not constrained very well by the observations and might deviate from the axis ratio of the larger scale disk. The resulting $R_{s,d}$ range for spheroidal models at a given inclination remains very similar. So this does not alter the conclusions inferred from Figures 4 and 5.

5. The non-gravitational gas dispersion component

The analysis of thin disks and spheroidal models indicates that non-gravitational forces might contribute significantly to the observed gas dispersion for radio galaxies. To constrain the minimal relative contribution of a non-gravitational dispersion component we plot in the top panel of Figure 6 the ratio of the observed dispersion and the maximum dispersion predicted by either disk or spheroidal models. The minimal ratio is typically between 1 and 2. There is a hint that the minimal ratio increases with axial ratio, i.e., for extended disks that are closer to face-on. This could indicate that the non-gravitational dispersion component does not have a random orientation with respect to the extended disk but is oriented preferentially along the spin axis of the extended disk. We explore this idea with two simple models. The models consist of two components: a thin circular rotating disk and a second component of non-gravitational motions. We assume equal contribution to the emission-line by the two components. In the 'isotropic model' the non-gravitational dispersion is isotropic (σ_{iso}) and the resulting total dispersion can be written as

$$\sigma_{obs}^2 = \sigma_{grav}^2 \sin^2 i + \sigma_{iso}^2 = 3\sigma_{grav}^2; \quad (6)$$

where σ_{grav} denotes the dispersion due to circular rotation as measured in the plane of the disk and i is the disk inclination. In the 'perpendicular model' the non-gravitational dispersion is assumed to be perpendicular to the plane of the disk:

$$\sigma_{obs}^2 = \sigma_{grav}^2 \sin^2 i + \sigma_{perp}^2 \cos^2 i; \quad (7)$$

The middle and bottom panels of Figure 6 show the ratios $\sigma_{iso} = \sigma_{grav}$ and $\sigma_{perp} = \sigma_{grav}$ as a function of disk axis ratio. The value of σ_{grav} is calculated as before from the thin disk models and σ_{iso} and σ_{perp} , respectively, are chosen so that σ_{obs} matches the observed value σ_g . The perpendicular model shows no trend between the dispersion ratio and disk inclination. The isotropic model shows a weak trend. This would not be expected in an isotropic scenario. On the other hand, the trend in Figure 6b is dominated by a few galaxies and is not really significant. For some galaxies the implied non-gravitational dispersion σ_{perp} is larger than $\sqrt{2} \sigma_{grav}$. In other words, the typical non-gravitational motions are larger than $\sqrt{2}$ times the typical circular rotation in those galaxies which suggests that

¹Note that in this case that the disk and spheroid do not have an identical surface density distribution.

some of the material might be unbound. However, the models are too simplistic to attach real significance to this result.

The fact that radio galaxies show an excess gas dispersion, while it appears to be absent in non-radio galaxies, possibly points to a link between non-gravitational motion and activity. The AGN could be a source of energy to drive the non-gravitational dispersion e.g., by coherent flows or turbulence. We do not have a direct measure of the kinetic energy output of the AGN to determine its correlation with the amount of non-gravitational dispersion present in the gas. Thus we resort to measures of the radiative energy output of the active nuclei as a proxy. Figure 7 shows R_{ord} as a function of total radio power for both radio and non-radio galaxies. As expected, the difference in excess dispersion for non-radio and radio galaxies is also present as a function of radio luminosity. However, there is no clear indication that larger non-gravitational motions occur in more powerful radio galaxies. We examined also the dependence of R_{ord} on radio core and nuclear emission-line luminosity for radio galaxies. No clear trends were found. Similarly, no trends were found between the ratios $\sigma_{\text{iso}} = \sigma_{\text{grav}}$ and $\sigma_{\text{perp}} = \sigma_{\text{grav}}$ with these three indicators of the radiative power of the active nucleus.

6. Caveats

Uncertainties in the flux profiles For three galaxies in our sample, NGC 3862, NGC 4374 and NGC 4486, we have both the STIS flux profiles and those derived from HST/WFPC2 PC-chip emission-line images which are available to us. The PC pixel size ($0.045''$) better samples the HST PSF FWHM ($0.1''$) compared to the STIS apertures. From the PC emission-line image, a narrower flux profile is inferred for NGC 3862 and NGC 4374, but a wider profile for NGC 4486, as compared to the flux profiles derived from the STIS data. Using the PC profiles in the thin disk modeling leads to increases in predicted gas velocity dispersion of 5%, 50% and 13% for NGC 3862, NGC 4374 and NGC 4486, respectively. Assuming that similar changes could be expected for the other sample galaxies, this does not change our conclusions.

Another possibility to consider is that we might have systematically overestimated the width of the emission-line flux profiles. If the flux in reality originates closer to the nucleus than in our models, it would naturally explain why the predicted dispersions are lower than observed. Figure 8 shows the radius inside which half of the flux from the intrinsic (i.e., unconvolved) flux profile is contained as a function of distance. The top panel shows the angular half light radius. For half light radii much less than the half light radius of the HST PSF, i.e., $0.05''$, it could well be that the intrinsic flux profile is in fact much narrower. Thus, the profile widths for NGC 2329, NGC 3862 and NGC 6251 should be considered upper limits. This implies that their predicted velocity dispersions should be considered lower limits as emission-line gas might be rotating closer to the black hole than in our models. However, there are two facts that argue against a general overestimate of the width of the flux profiles for all galaxies. First, we find no trend of narrower emission-line flux profiles with increasing dispersion ratios. Second, such a scenario cannot explain the correlation between disk inclination and dispersion ratio. A separate question is whether we are resolving the flux profile at larger distances as well as nearby. This issue is relevant for comparing

the properties of the radio galaxies and non-radio galaxies, since the former sample has a larger average distance. The bottom panel of Figure 8 suggests that this distance offset is not inducing the difference in excess dispersion, since there is no trend between the physical half light radius and distance.

Finally, what kind of emission-line flux profile is needed to obtain the observed gas velocity dispersions gravitationally? To first approximation $\frac{2}{g} M = R_{\text{ux}}$ where R_{ux} is the typical radius of the flux profile (e.g., the half light radius). Figure 4 shows that for radio galaxies R_{ux} needs to decrease by a factor of about 2 up to 100 to have a model with a black hole mass according to the M relation account for the observed gas dispersion. Figure 8 shows that the emission-line flux profile for radio galaxies typically has a half light radius which is 2 times the radius of the PSF. In conclusion, the emission-line profile for radio galaxies needs to be fully unresolved in general to account for the observed gas velocity dispersion gravitationally. This is ruled out by the observations.

Uncertainties in the location of the black hole The spatial flux distribution in the direction of the slit length allows us to precisely locate the nucleus along this direction (assuming it coincides with the peak of the emission-line flux, cf. Section 2). But the nucleus was assumed to be at the center of the slit in the direction of the slit width. This is a reasonable assumption (see Section 2). We determined that a $0.05^{\text{''}}$ displacement in this direction changes the predicted velocity dispersion by $< 20\%$ for the thin disk models. This does not affect our conclusions.

Does the M relation underestimate BH masses? One might account for the excess gas dispersion within the purely gravitational models, seen particularly for radio galaxies, by assuming that the BH mass from the M relation underestimates the true BH mass. However, this requires increases in BH masses that are too large to be credible for the following reasons. First, comparison of Figure 2 and 3 shows that detailed estimates of BH masses from gas rotation velocity modeling do not show any indication for BH masses that are systematically larger than those inferred from the M relation. (This is a somewhat circular argument as some of the BH mass measurements from gas were used to determine the M relation. Nevertheless, such large BH masses would imply velocity gradients which are larger than observed.) Second, the trend of an increasing R_{opt} with decreasing disk inclination is not expected if the excess dispersion is due to underestimated BH masses. The dependence of BH mass on stellar dispersion is sometimes claimed to be steeper than used here (e.g., Ferrarese 2002). However, this amounts to at most 50% larger BH masses and such uncertainties will not affect our results on excess gas dispersions. Lastly, it has been argued that M correlates equally well with host luminosity as with σ (e.g., Marconi & Hunt 2002). This might mean that the M relation underestimates M at the high end. The reason is that Brightest Cluster Galaxies (BCGs) fall in this region. The BCGs are exceedingly luminous for their stellar dispersion which is typically above 270 km s^{-1} (Fisher, Illingworth & Franx 1995). If true, it is very unlikely that this will affect our results because the galaxies in our sample with the largest excess in stellar dispersion compared to gravitational models all have stellar dispersions between 190 km s^{-1} and 270 km s^{-1} (cf., Figure 9).

Are thin disk models plausible? It was found that for most of the normal galaxies in our sample the nuclear gas dispersions are reasonably well fit by thin disk models containing BHs that

follow the M relation. But the full emission lines shapes contain additional information on the line of sight velocity distribution (LOSVD) and can further constrain the plausibility of the models. We used the thin disk models to calculate the full LOSVD for the normal galaxies in the sample. Inspection of the data shows a qualitative agreement between predicted and observed LOSVDs. A general property of the LOSVD of thin disk models is a tendency for being double-peaked. In some cases the predicted double peakedness seems slightly too pronounced to be consistent with the data. But it is possible that the predicted peaks have in reality been broadened away by additional velocity dispersion contributions. For example, the gas could be collisionless but orbit in a somewhat more three-dimensional distribution than a disk (as in the models of Section 4), or it could have a small additional non-gravitational contribution (as in the models of Section 5). Overall, the signal-to-noise ratio of the data and the blending of the H + [N II] lines make it difficult to draw strong conclusions from the observed line shapes.

Could an unaccounted broad H component in radio galaxies influence our results? The flux from which the velocity dispersions are measured is usually dominated by the flux from the forbidden [N II] and [S II] lines, especially the [N II] 6584 line and not the H line. Furthermore, we ensured to correct for the presence of broad H if it was clearly detected. This broad component is likely arising from a broad-line region which is located much closer to the nucleus than the narrow component that we model here. Noel-Storr et al. (2003) found tentative indications that a broad line, not readily seen by eye, could be present in eight of the radio galaxies in our sample (Table 1). In these cases they performed fits to the H + [N II], [S II] complex assuming the permitted H line has both a narrow and a broad component. We redid the thin disk modeling for these eight galaxies taking into account the tentative broad component in measuring the velocity dispersion and emission-line profile of the narrow component. This resulted in decreases of R_{ord} by at most 20% and a median decrease of 9%. Thus these eight galaxies do not change the overall results obtained together with the 13 other radio galaxies. Lastly, the dispersion in the extended disk are in many radio galaxies above those expected from instrumental effects and differential rotation over the aperture (e.g., Noel-Storr et al. 2003). This strengthens the idea that the excess dispersions are not due to a nuclear broad line region.

Gaussian fit versus true second velocity moment. For the thin disk models we compared the predicted second moment of a Gaussian fit to the full line of sight velocity distribution (LOSVD) to the observed Gaussian fit. By contrast, in the analysis of more spheroidal distributions, R_{sd} is the ratio of the true second moments. Thus we assume that the ratio of the true second moments and the ratio of the Gaussian-fit moments do not differ significantly. It is not straightforward to test this assumption quantitatively, since the line profiles are not straightforward to calculate for the spheroidal models. However, we believe that the errors thus introduced are unlikely to exceed several tens of percent (van der Marel & Franx 1993). This is insufficient to affect any of our conclusions. Also, it seems unlikely that a difference in these ratios would affect our main result that there is a systematic difference in nuclear dispersions between radio and non-radio galaxies.

Dependence of the stellar dispersion on inclination. In our models we have assumed that the BH mass is uniquely determined by the stellar velocity dispersion. However, this can only be approximately true in reality. There must be some intrinsic scatter in the M relation, if only because the observed velocity dispersion of a galaxy generally depends on the inclination

under which the galaxy is viewed, whereas the BH mass does not. This could be important in the context of our results. The four galaxies for which thin disk models fit the observed gas dispersions most poorly have below-average inclinations, in addition to being radio galaxies (see Figure 3). It is therefore important to study the relation between stellar velocity dispersion and inclination in some more detail.

To support its shape, an oblate stellar system must on average have more pressure (σ^2) parallel to the equatorial plane ($\frac{\sigma_k^2}{\sigma^2} = \frac{\overline{v^2} + \overline{v_R^2}}{2}$) than perpendicular to it ($\frac{\sigma_{\perp}^2}{\sigma^2} = \frac{\overline{v_z^2}}{2}$). Therefore, it will generally have a lower line-of-sight velocity dispersion when viewed face-on than when viewed edge-on. The tensor virial theorem (Binney & Tremaine 1986) gives the ratio of the pressures when integrated over the entire galaxy as

$$\left(\frac{\sigma_k}{\sigma_{\perp}}\right)^2 = \frac{\frac{1}{2} \frac{1 - e^2}{1 + e^2} \frac{\arcsin e}{e}}{1 - \frac{1}{2} \frac{1 - e^2}{1 + e^2} \frac{\arcsin e}{e}}; \quad e^2 = 1 - q_{\perp}^2 \quad (8)$$

where q_{\perp} is the intrinsic axial ratio. For example, this gives $\frac{\sigma_k}{\sigma_{\perp}} = 1$ for a spherical galaxy and $\frac{\sigma_k}{\sigma_{\perp}} = 1.34$ for a galaxy with $q = 0.5$. If one were to observe a galaxy with an aperture of infinite size, and if the galaxy had $\overline{v^2} = \overline{v_R^2}$ at all positions in the galaxy, then the ratio of the measured dispersion when viewed edge-on and face-on, respectively, would be equal to $\frac{\sigma_k}{\sigma_{\perp}}$. However, these requirements are not generally met for real galaxies and real observations. There is no reason why galaxies should have $\overline{v^2} = \overline{v_R^2} = 1$, and observational constraints on this ratio remain scarce (e.g., Gebhardt et al. 2003). Also, velocity dispersion measurements are generally restricted to the central region of the galaxy and/or a specific axis (most often the major axis) and do not integrate over the entire galaxy. So the true dependence of the observed stellar velocity dispersion on the inclination angle can only be addressed with detailed three-integral stellar dynamical models (e.g., Gebhardt et al. 2003; Cappellari et al. 2005b), which are outside the scope of the present work. Nonetheless, the tensor virial theorem does provide useful order-of-magnitude guidance. Almost all elliptical galaxies have axial ratios $q > 0.5$ (Franx, Illingworth & de Zeeuw 1991; Tremblay & Merritt 1995). Therefore, one might expect that inclination effects cause a variation of order $\sim 15\%$ (~ 0.06 dex) in the observed velocity dispersion of galaxies of otherwise identical properties.

An alternative way to constrain the inclination dependence of the velocity dispersion is through the scatter in several well-known relations. The velocity dispersion correlates strongly with galaxy luminosity (the Faber-Jackson relation; e.g., Dressler et al. 1987), with BH mass (the M - σ relation), and with galaxy mass-to-light ratio M/L (Cappellari et al. 2005b). None of the latter quantities depends on the viewing angle of the observations, while the velocity dispersion does. Therefore, the observed scatter in these relations sets an upper limit to the RMS variation that the inclination might induce in the observed velocity dispersion. The limits are $0.25=3.50 = 0.072$ dex from the Faber-Jackson relation (Dressler et al. 1987), $0.30=4.02 = 0.075$ dex from the M - σ relation (Tremaine et al. 2002), and $0.07=0.82 = 0.083$ dex from the relation with M/L (Cappellari et al. 2005b). These results are all in reasonable agreement with the expectation from the virial theorem (despite the fact that each of these relations is likely to have other sources of intrinsic scatter as well). Lastly, direct estimates of the dispersion anisotropy in giant ellipticals from detailed three-integral stellar dynamical models indicate a change of ~ 0.05 dex in stellar dispersion for face-on

and edge-on viewing angles (Cappellari et al. 2005a). Given that rotational velocities contribute typically less than 10% to the second moment of giant ellipticals this lends further support for the estimates based on global relations for the dependence of the stellar dispersion on inclination.

To obtain more specific information for the actual galaxies in our sample we plot their Faber-Jackson relation in Figure 9. The four galaxies with dust/gas disk inclinations $i < 40^\circ$ are indicated with special symbols. If the disks reside in the equatorial plane of the galaxies, then the disk inclinations are identical to the galaxy inclinations. One would then expect the galaxies with $i < 40^\circ$ to have relatively low stellar velocity dispersions for their luminosity. This is exactly what the figure shows. The galaxies with $i < 40^\circ$ seem to lie $\sim 17\%$ (0.079 dex) below the average relation between galaxy magnitude and stellar dispersion. This agrees to lowest order with the expectation from the tensor virial theorem and the scatter in well-known correlations.

So there is theoretical and observational support for the idea that the observed stellar velocity dispersion depends on the galaxy inclination angle. By using the M_{BH} relation to estimate the BH mass one is therefore likely to underestimate the BH mass of galaxies with relatively low inclinations. For the galaxies in our sample with $i < 40^\circ$ we may have underestimated the BH mass by a factor $0.83^{4.02} = 2.1$. The gas dispersions predicted by our thin disk models will then be too low by a factor of $\sqrt{2.1} = 1.4$. Applying this correction to the predicted gas dispersions for the $i < 40^\circ$ galaxies in e.g., Figure 3 somewhat reduces the discrepancy between the observed and predicted gas dispersions for these galaxies. Nonetheless, for all four of the galaxies the observed gas dispersions remain well in excess over those predicted by the thin disk models. So our conclusion that radio galaxies have a contribution from non-gravitational motions in their central gas dynamics remains unaffected.

7. Conclusions & Discussion

We have analyzed HST/STIS observations of a sample of 27 galaxies. The nuclear velocity dispersion of the gas in a STIS aperture of $0.1''$ (i.e., scales of tens of parsecs) generally exceeds the large-scale stellar velocity dispersion of the galaxy. This is qualitatively consistent with the presence of central BHs, but raises the questions whether the excess gas dispersion is of gravitational or non-gravitational origin and whether the implied BH masses are consistent with our current understanding of BH demography. To address these issues we have constructed purely gravitational axisymmetric dynamical models for the gas, both thin disk models and models with more general axis ratios and velocity anisotropies. This has yielded the following conclusions:

For the normal galaxies in the sample (i.e., without large-scale radio-jets) the nuclear gas dispersions are adequately reproduced by models that have purely gravitational motion and BHs that follow the M_{BH} relation. Among the purely gravitational models we cannot generally discriminate between thin disk models and vertically extended models. The former might seem preferred theoretically because they represent a longer-term equilibrium configuration for the gas. However, in some cases it is unclear if the observed line profiles are consistent with the double-peaked structure that is generally predicted by thin disk models.

The nuclear gas dispersions observed for the radio galaxies generally exceed those predicted by models with only gravitational motions in either a thin disk or a more spheroidal gas distribution. We attribute this to the presence of non-gravitational motions in the gas that are similar to or larger than the gravitational motions. The non-gravitational dispersion is consistent with being either isotropic or perpendicular to the extended gas and dust disks. The non-gravitational motions are presumably driven by the active galactic nucleus (AGN), but we do not find a relation between the radiative output of the AGN and the non-gravitational dispersion.

Given the uncertainties about the dynamical state of the gas, it is not possible to uniquely determine the BH mass for each galaxy from its nuclear gas dispersion. However, for the sample as a whole the observed dispersions do not provide evidence for significant deviations from the $M_{\text{BH}} - \sigma$ relation in either active or non-active elliptical galaxies. In no case is the observed nuclear gas dispersion so low that it puts an upper limit on the BH mass that is significantly below the $M_{\text{BH}} - \sigma$ relation.

For the normal, i.e., non-radio galaxies, one should note that the success of purely gravitational models does not imply that there are no alternative models that can fit the data. For example, it cannot be ruled out that in reality there is a non-gravitational component to the gas motions, and that the BH masses in these galaxies are below the $M_{\text{BH}} - \sigma$ relation. Some models in the literature, such as those published for IC 1459 (Cappellari et al. 2002) fall in this category. Nevertheless, if one is willing to assume a priori that the BH masses of all elliptical galaxies follow the $M_{\text{BH}} - \sigma$ relation, then one can turn the argument around and conclude that normal elliptical galaxies do not have a very significant non-gravitational component in their gas motions. The absence of excess dispersion in non-radio galaxies is corroborated by the fact that the BH mass estimates for this sample by itself yield a relation in good agreement with the $M_{\text{BH}} - \sigma$ relation (e.g., Figure 3). It is interesting to note in this context that a similarly good correspondence between BH masses from gas dispersions and from the $M_{\text{BH}} - \sigma$ relation was found for non-active early-type spiral galaxies by Sarzi et al. (2002).

For the low-luminosity radio galaxies in our sample there is also other evidence, besides the dynamical evidence presented here, for non-axisymmetric gas distributions with turbulent motion. The core emission-line luminosity of these galaxies correlates with the radio and optical core luminosity which are both most likely due to synchrotron emission from the jet (e.g., Chiaberge et al. 1999; Verdoes Kleijn et al. 2002). This correlation could mean that the emission-line luminosity is driven by jet photo-ionization. It then implies covering factors of ~ 0.3 and hence thick disks (Capetti 2005). Alternatively, the correlation could indicate that the gas is excited by shocks induced by jet-gas interactions.

Although it is mostly the radio galaxies that show significant excess dispersion over a purely gravitational model, there is one normal galaxy for which this is the case too: IC 989. It should be noted though that for this particular galaxy the error of 33 km s^{-1} on the stellar dispersion $\sigma_s = 176 \text{ km s}^{-1}$ is larger than typical for the sample. The predicted gas dispersion can be increased by a factor ~ 4 by simply varying σ_s within its 1- σ confidence range. Also, the predicted gas dispersion could go up by up to a factor ~ 2 if the unknown inclination of the purported gas

disk is closer to edge-on than the default value of 60 that we assumed. So the evidence for non-gravitational gas motions in the normal galaxy IC 989 is not strong.

Finally, we note that it is the sample of relatively close to face-on ($i < 40^\circ$) gas disks which reveal most clearly an excess dispersion compared to a purely gravitational model. Unfortunately, this face-on group only contains radio galaxies. However, a statistically significant difference between the excess dispersion in radio and non-radio galaxies remains when one excludes galaxies with $i < 40^\circ$ gas disks from the analysis. Nevertheless, a good test of the dichotomy found in this paper will be the modeling of gas disks at lower inclinations also in non-radio galaxies. Such data is not available currently.

The evidence for non-gravitational gas motions in radio galaxies makes the gas dispersion unsuited for dynamical mass estimates in this class of galaxies. It would be interesting to establish more generally whether dynamical mass estimates from gas velocities, including rotation curves, are robust. This would require comparisons of BH masses from independent indicators (e.g., stellar and gas kinematics) within the same galaxy. Such a comparison has been performed for a radio galaxy (NGC 4335, Verdoes Kleijn et al. 2002) and a non-radio galaxy (Cappellari et al. 2002). Unfortunately, in both cases the stellar dynamical evidence is too inconclusive to reach firm conclusions. But it does appear in both cases that the BH mass implied by thin disk models for the gas rotation curves is lower than would otherwise have been expected, either from stellar kinematics or from the M – σ relation. This suggests that the gas might be moving slower than the circular velocity, as would be expected for example if there were asymmetric drift in the gas. This occurs for gas distributions that are dynamically hotter than a thin disk. More independent BH mass evaluations from gas and other tracers, both for normal and active galaxies, would be quite valuable to shed more light on these issues.

Support for this work was provided by a grant associated with program GO-9163 from the Space Telescope Science Institute, which is operated by AURA, Inc., under NASA contract NAS5-26555. This paper made use of the LEDA database (see <http://leda.univ-lyon1.fr>). We thank the anonymous referees for their constructive comments. We thank the first referee in particular for drawing our attention to the dependence of stellar velocity dispersion on galaxy inclination (see the discussion in Section 6).

REFERENCES

- Allen G. A., Dopita M. A., Tsvetanov Z. I., 1998, *ApJ*, 493, 571
- Barth, A. J., Sarzi, M., Rix, H., Ho, L. C., Filippenko, A. V., & Sargent, W. L. W. 2001, *ApJ*, 555, 685
- Barth, A. J. 2004, *Coevolution of Black Holes and Galaxies*, 21
- Becker, R. H., White, R. L., & Helfand, D. J. 1995, *ApJ*, 450, 559
- Binney, J. 1980, *MNRAS*, 190, 873
- Binney, J. J., & Tremaine, S. D. 1987, *Galactic Dynamics* (Princeton: Princeton Univ. Press)

- de Bruijne, J. H. J., van der Marel, R. P., & de Zeeuw, P. T. 1996, *MNRAS*, 282, 909
- Cappellari, M., Verolme, E. K., van der Marel, R. P., Kleijn, G. A. V., Illingworth, G. D., Franx, M., Carollo, C. M., & de Zeeuw, P. T. 2002, *ApJ*, 578, 787
- Cappellari, M., et al., 2005a, in "Nearly Normal Galaxies in a Λ CDM Universe", in press, astro-ph/0509470
- Cappellari, M., et al., 2005b, submitted to *MNRAS*, astro-ph/0505042
- Chiaberge, M., Capetti, A., & Celotti, A. 1999, *A & A*, 349, 77
- Capetti, A., Verdoes Kleijn, G. A., Chiaberge, M., 2005, *A & A*, 439, 395
- Dojta, M. A., Koratkar, A. P., Allen, M. G., Tsvetanov, Z. I., Ford, H. C., Bicknell, D., Resse, L. L., & Condon, J. J. 1978, *ApJS*, 36, 53
- Dressler, A., Faber, S. M., Burstein, D., Davies, R. L., Lynden-Bell, D., Terlevich, R. J., & Wegner, G. 1987, *ApJ*, 313, 42
- Faber S. M., et al., 1989, *ApJS*, 69, 763
- Ferrarese L. C., Ford H. C., Jaffe W., 1996, *ApJ*, 470, 444
- Ferrarese, L. C., & Ford, H. C. 1999, *ApJ*, 515, 583
- Ferrarese L. C., Merritt D., 2000, *ApJ*, 539, L9
- Fisher D., Illingworth G. D., Franx M., 1995, *ApJ*, 438, 539
- Franx M., Illingworth G. D., de Zeeuw P. T., 1991, *ApJ*, 383, 112
- Gebhardt, K., et al. 1996, *AJ*, 112, 105
- Gebhardt K., et al., 2000, *ApJ*, 539, L13
- Gebhardt K., et al., 2003, *ApJ*, 583, 92
- Gri th, M. R., Wright, A. E., Burke, B. F., & Ekers, R. D. 1994, *ApJS*, 90, 179
- Grupe, D. & Mathur, S. 2004, *ApJ*, 606, L41
- Hamas, R. J., et al. 1994, *ApJ*, 435, L35
- Ghez, A. M., et al. 2003, *ApJ*, 586, L127
- Goudfrooij P., Hansen L., Jorgensen H. E., Norgaard-Nielsen H. J., 1994 *A & AS*, 105, 341
- Habe, A. & Ikeuchi, S. 1985, *ApJ*, 289, 540
- aring, N., & Rix, H. 2004, *ApJ*, 604, L89
- Ho, Filippenko & Sargent, 1997, *ApJ*, 487, 568
- Koprolin, W., Zeilinger, W. W., 2000 *A & AS*, 145, 71
- Kormendy, J. & Richstone, D. 1995, *ARA & A*, 33, 581
- Kormendy J., Gebhardt K., 2001, in *The 20th Texas Symposium on Relativistic Astrophysics*, eds. H. Martel, J. C. Wheeler, *IP*, 363
- Laine, S., van der Marel, R. P., Lauer, T. R., Postman, M., O'Dea, C. P., & Owen, F. N. 2003, *AJ*, 125, 478

- M acchetto F D , et al, 1996, A & A S, 120, 463
- M acchetto F D ., M arconi A ., Axon D J., Capetti A ., Sparks W ., C rane P ., 1997, ApJ 489, 579
- M aciejew ski W ., Binney J., 2001, M N R A S, 323, 831
- M arconi A ., Hunt L.K ., 2003, ApJ, 589, L21
- M auch, T ., M urphy, T ., B uttery, H . J., Curran, J., H unstead, R . W ., P iestrzynski, B ., R obertson, J.G ., & S adler, E.M . 2003, M N R A S, 342, 1117
- Noel-Storr, J., Baum , S.A ., Verdoes K leijn, G ., van der M arel, R . P ., O 'D ea, C . P ., de Zeeuw , P . T ., & C arollo, C . M . 2003, ApJS, 148, 419
- Phillips M M ., Jenkins C R ., D opita M A ., S adler E M ., B inette L ., 1986, A J, 91, 1062
- Soltan, A . 1982, M N R A S, 200, 115
- Sarzi et al, 2002, ApJ, 567, 237
- Schodel, R ., O tt, T ., G enzel, R ., Eckart, A ., M ouaw ad, N ., & A lexander, T . 2003, ApJ, 596, 1015
- Tonry, J.L ., et al, 2001, ApJ, 546, 681
- Tran, H . D ., T svetanov, Z ., Ford, H . C ., Davies, J., Ja e, W ., van den Bosch, F . C ., & Rest, A . 2001, A J, 121, 2928
- Trem aine et al, 2002, ApJ, 574, 740
- Trem blay B ., & M erritt D . 1995, A J, 110, 1039
- van der M arel R P ., van den Bosch F C ., 1998, A J, 116, 2220
- van der M arel, R . P ., & Franx, M . 1993, ApJ, 407, 525
- van D okkum & Franx 1995,
- Verdoes K leijn, G . A ., van der M arel, R . P ., C arollo, C . M ., & de Zeeuw , P . T . 2000, A J, 120, 1221
- Verdoes K leijn G A ., van der M arel R P ., de Zeeuw P.T ., Noel-Storr J., Baum S A ., 2002, A J, 124, 2524
- W hite, R . L . & Becker, R . H . 1992, ApJS, 79, 331
- W hite, S.D . M ., D avis, M ., H uchra, J., & Latham , D . 1983, M N R A S, 203, 701
- W right, A . & O trupcek, R ., Parkes C atalogue, 1990, ATNF
- Zeilinger W W ., et al, 1996, A & A S, 120, 257

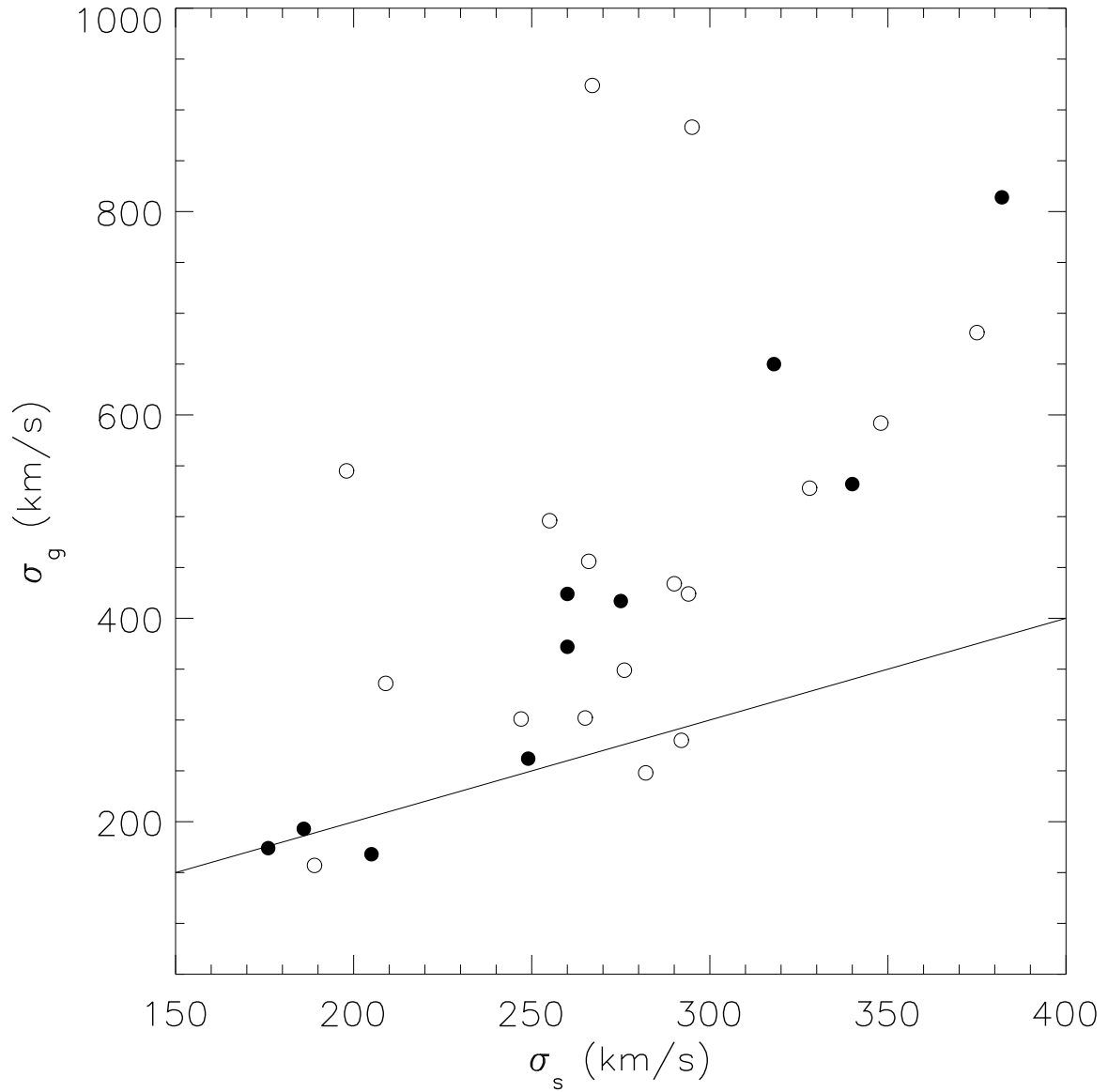


Fig. 1. | HST measured nuclear gas velocity dispersion versus large-scale stellar velocity dispersion for our sample galaxies. Open symbols indicate FR I-type radio galaxies, while solid symbols indicate galaxies without large-scale radio jets. Most galaxies have nuclear gas dispersions larger than their stellar dispersions (the equality of the two being indicated by the line).

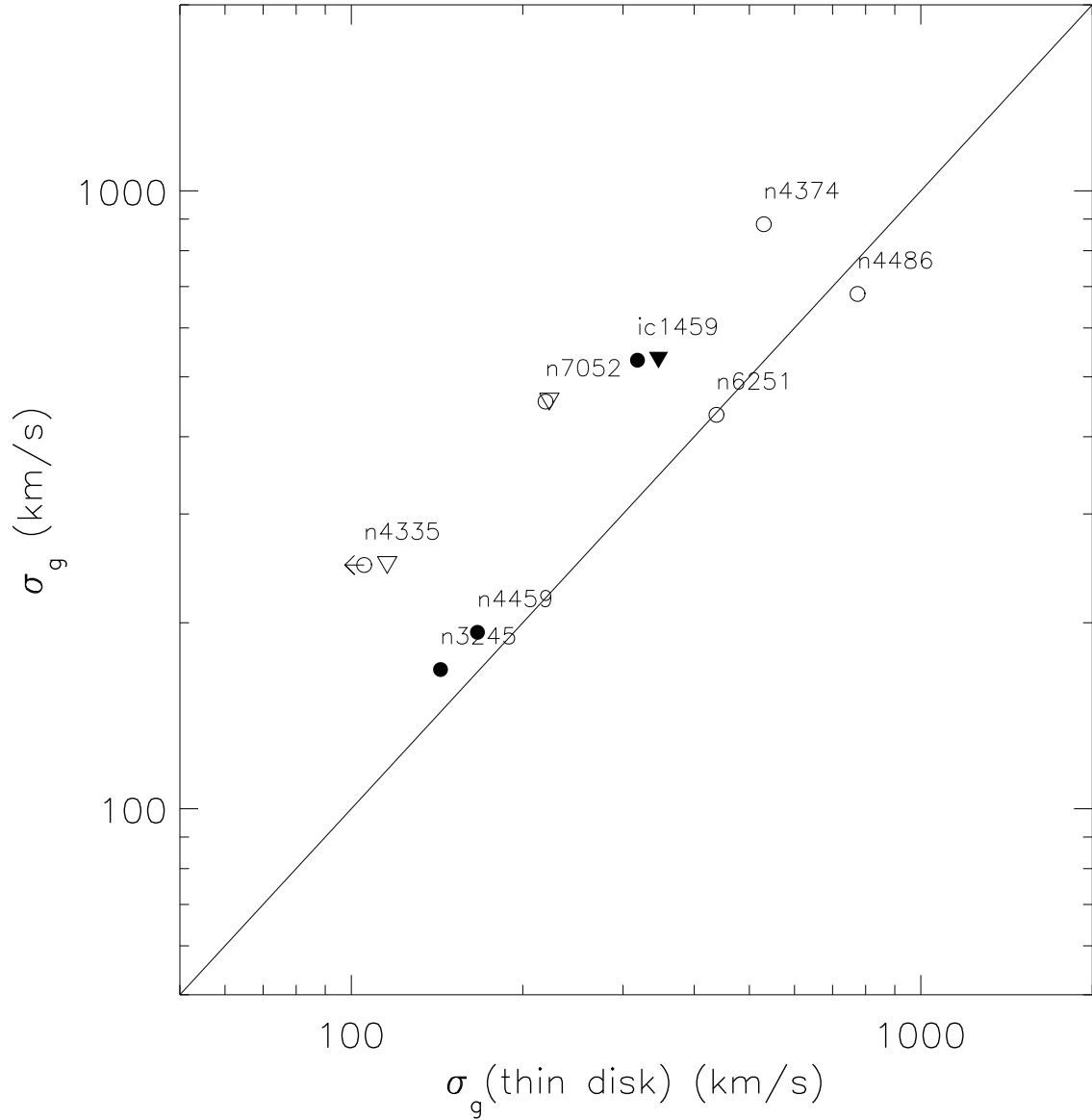


Fig. 2. | Observed gas velocity dispersion versus predicted gas velocity dispersion for a thin disk model. We use the BH masses and inclinations inferred from detailed models for the gas rotation velocities available in the literature (see Tables 1 and 2). Open symbols indicate FR I-type radio galaxies, while filled circles indicate galaxies without large-scale radio jets. Circles indicate results from the thin disk models that neglect the contribution of the stellar mass to the gravitational potential. Triangles show the predictions when this simplification is omitted, for the three galaxies for which we published detailed gas modeling previously. The difference between the two model approaches is $< 10\%$.

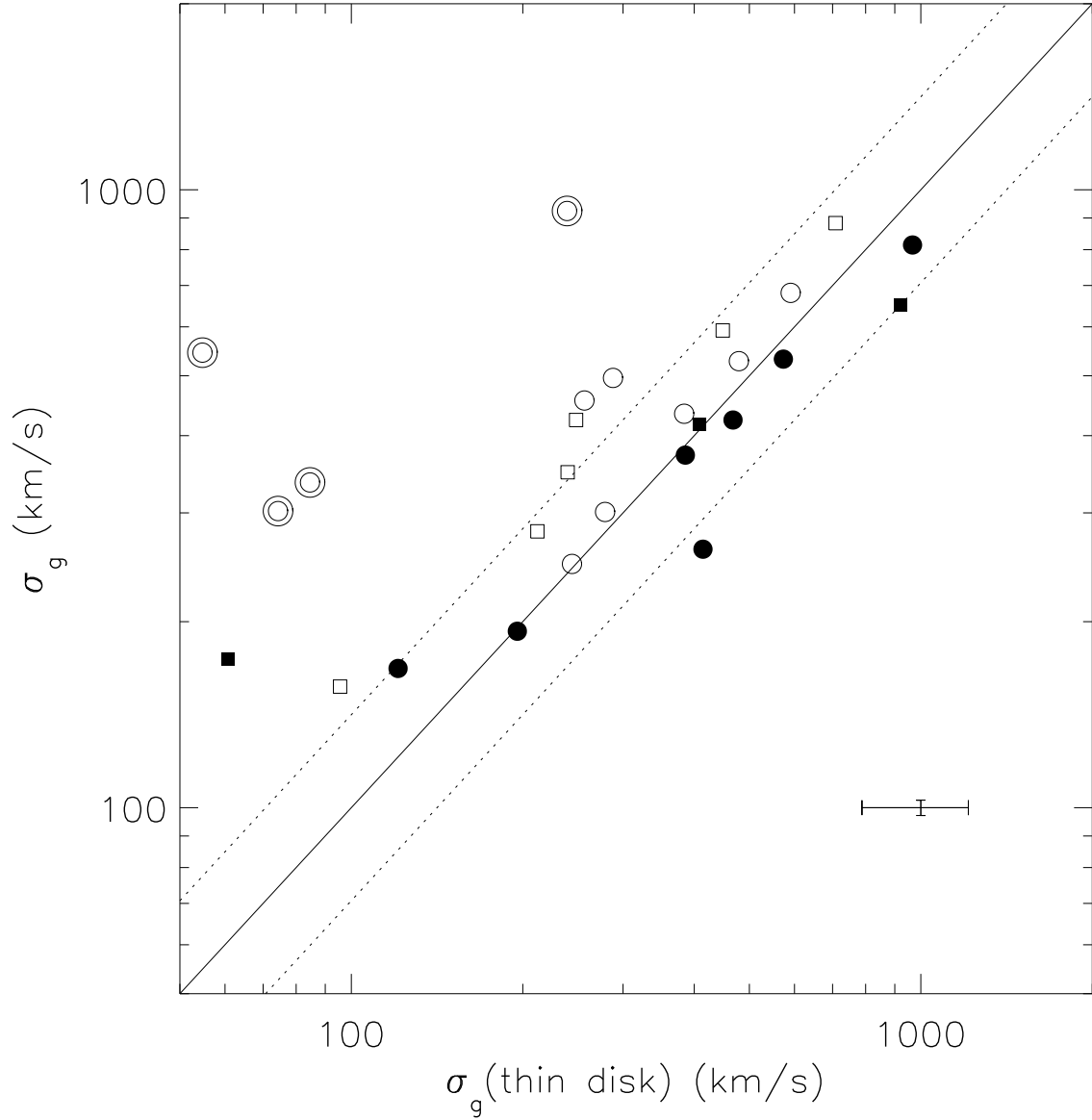


Fig. 3. The observed gas velocity dispersion σ_g as a function of predicted velocity dispersion for an infinitely thin gas disk in circular rotation around a BH with mass M according to the M relation. Radio galaxies are shown as open symbols and galaxies without large-scale radio jets as filled symbols. Squares indicate galaxies for which the disk inclination is unknown and assumed to be 60° . Galaxies with disk inclination $i < 40^\circ$ are indicated by double circles. The typical measurement errors are indicated in the lower right corner. The dashed and solid lines indicate $\sigma_g(\text{model}) = (\overline{p}^{-2} \pm 1; \overline{p}^{-2}) \sigma_g(\text{obs})$, respectively, to facilitate comparison to the M relation and its 0.3 dex scatter in BH mass.

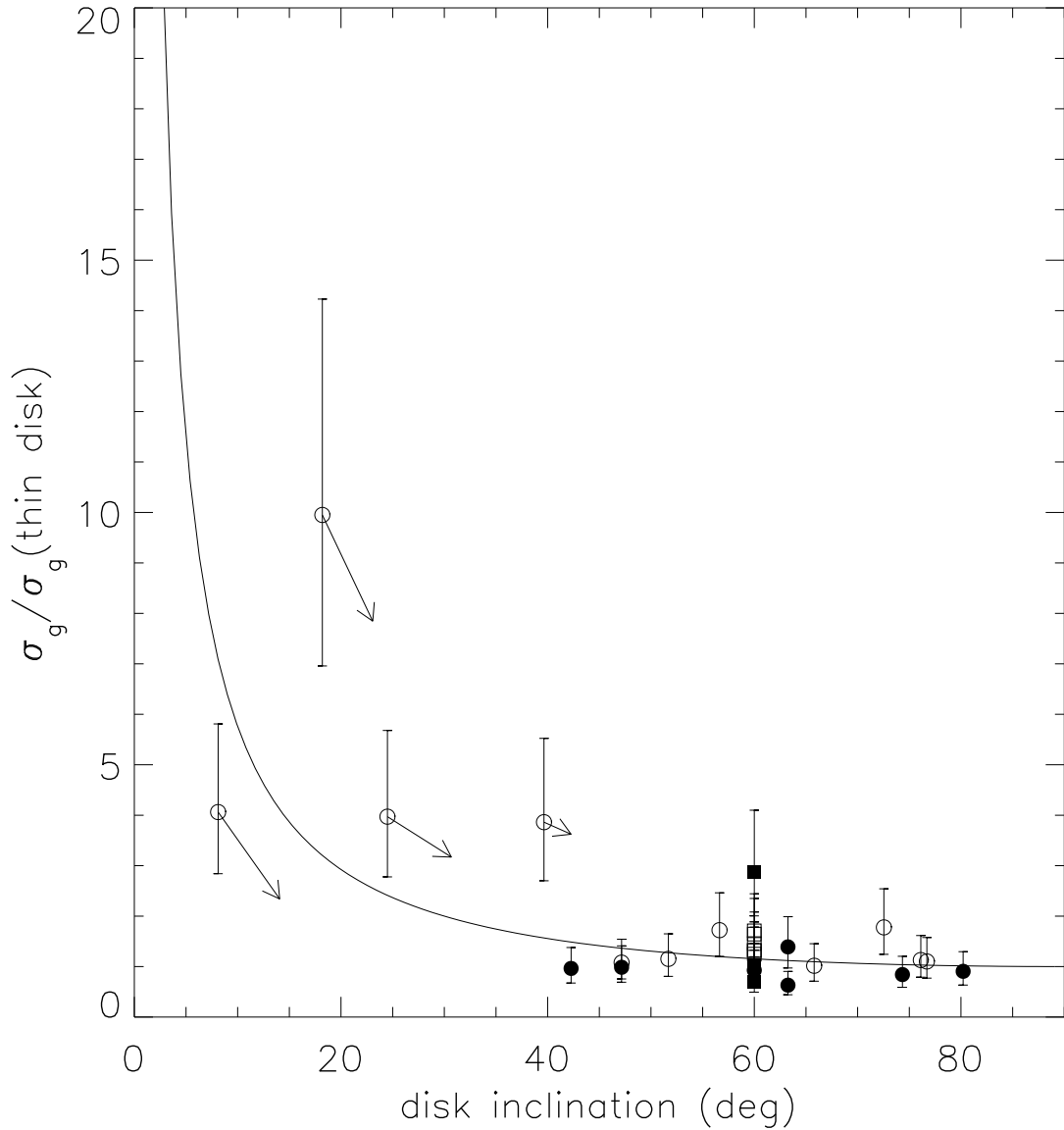


Fig. 4. | Ratio of observed and predicted gas dispersions as a function of gas disk inclination. The predicted dispersion is assumed to be caused by the circular rotation in a thin disk around a BH according to the M relation. The error bars take into account the 0.3 dex intrinsic scatter in the M relation, and typical errors due to aperture differences and dispersion measurement errors. The four arrows indicate where points will move if disk inclinations were underestimated within the measurement errors for close to face-on disks. Radio galaxies (open symbols) have a systematically larger dispersion ratio than non-radio galaxies (filled symbols). The squares indicate galaxies for which the dust does not provide a constraint on the gas disk inclination (placed at a fiducial inclination of 60°). If the assumed disk inclinations are incorrect, and the observed gas is actually edge-on in all galaxies, then we would have expected the ratios to lie along the solid line $\sin^{-1} i$. Since many points lie above this line, inclination errors cannot be the (sole) explanation of the observed trend.

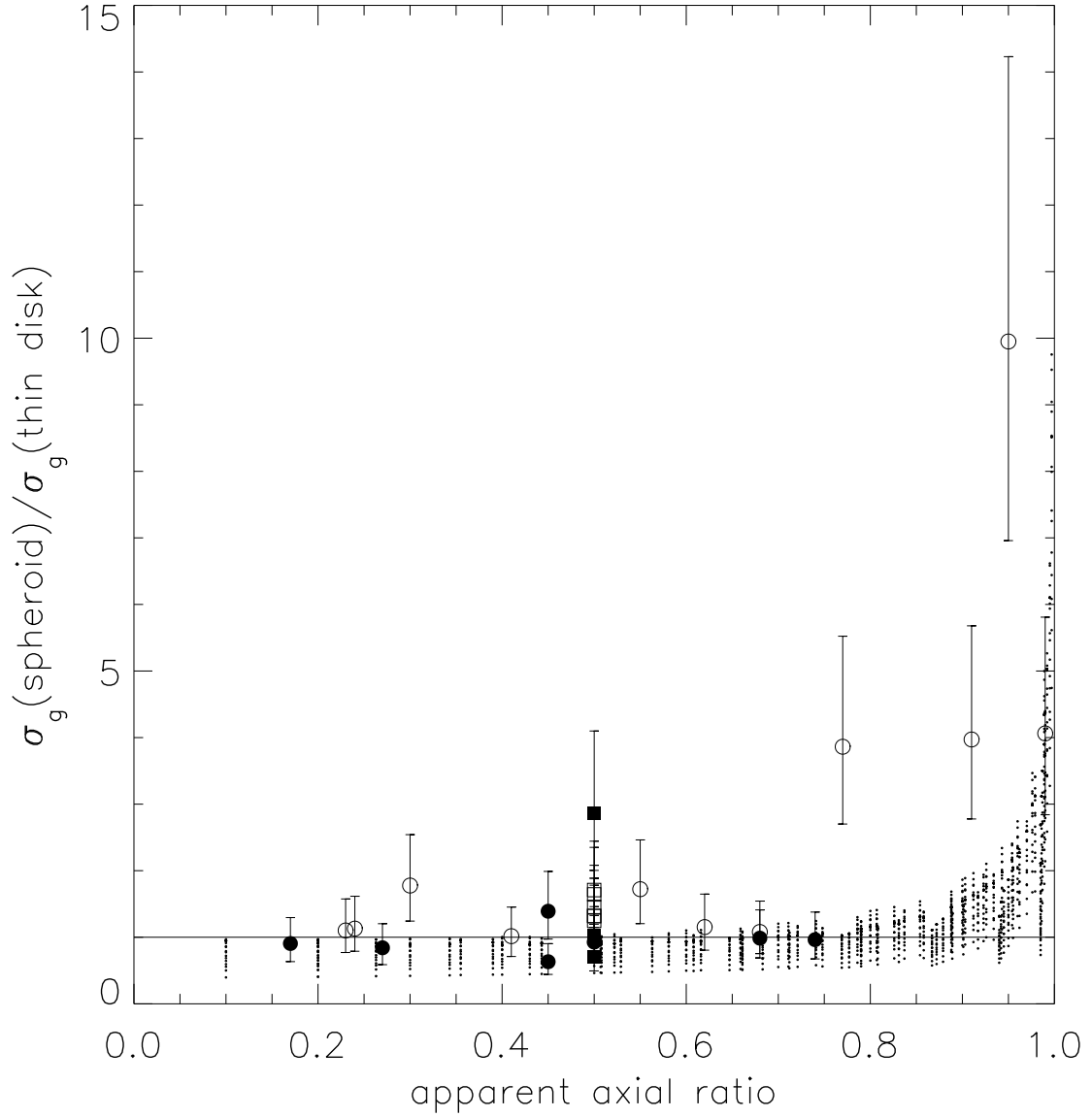


Fig. 5. The ratio of the velocity dispersion for a collisionless spheroid divided by that of a thin disk with identical projected surface density profile, as a function of apparent axis ratio. The small dots indicate spheroid models with varying intrinsic axis ratios, powerlaw density slopes and velocity dispersion anisotropies. The ratios of observed velocity dispersions and dispersion predicted by thin disk models from Figure 4 are overplotted. Symbols are as in Figure 4.

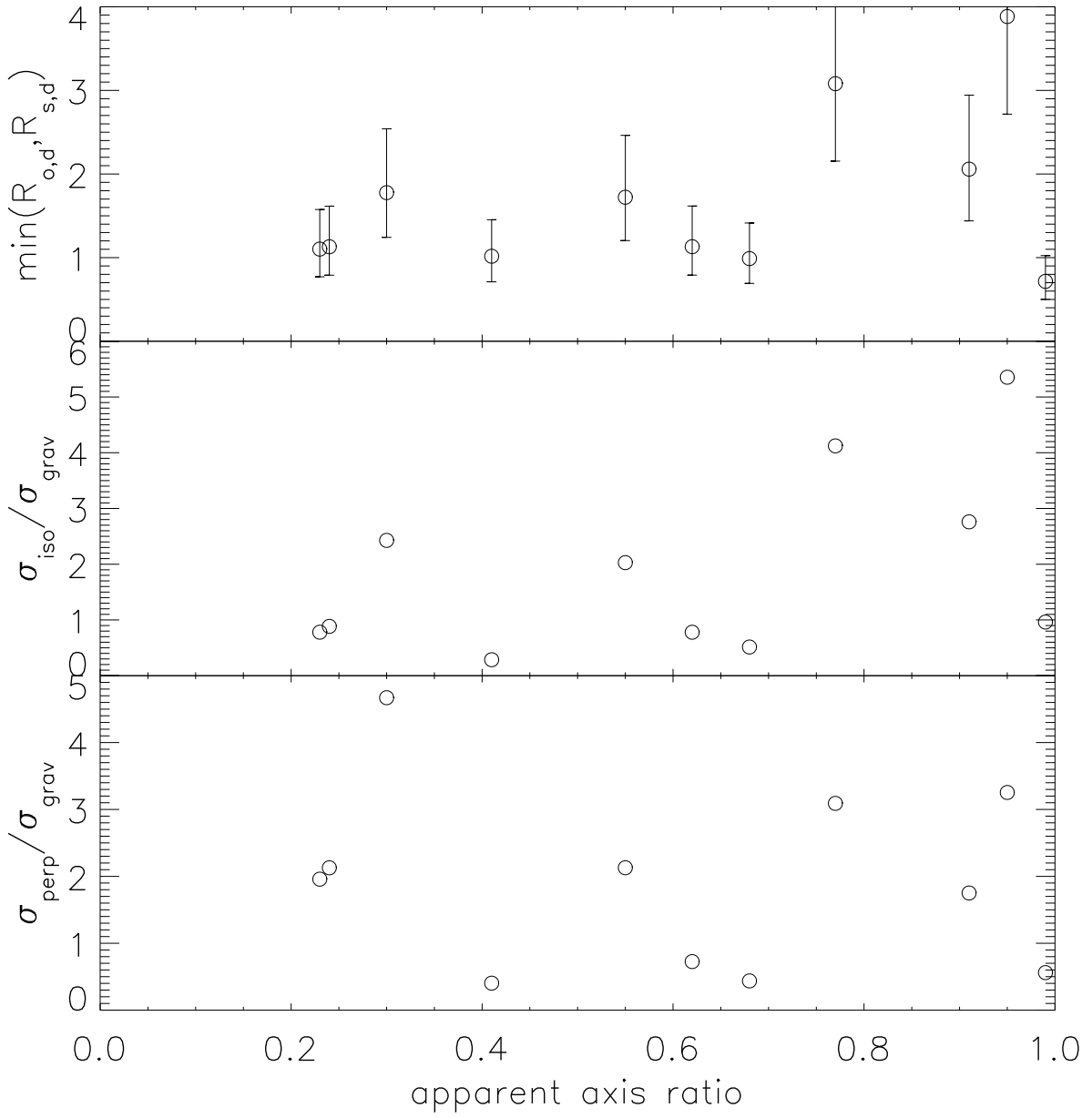


Fig. 6. | Top: The ratio between the observed dispersion and the maximum dispersion expected from spheroids or thin disks for radio galaxies with determined inclinations. The ratio is systematically above 1. Middle: The ratio of non-gravitational dispersion σ_{iso} and gravitational dispersion σ_{grav} for a two component gas model which matches the observed dispersion. The model has a circular thin gas disk which causes σ_{grav} measured in the plane of the disk and a non-gravitational component with an isotropic gas dispersion σ_{iso} . Bottom: Similar to middle plot, but now the non-gravitational dispersion component is assumed to be perpendicular to the gas disk.

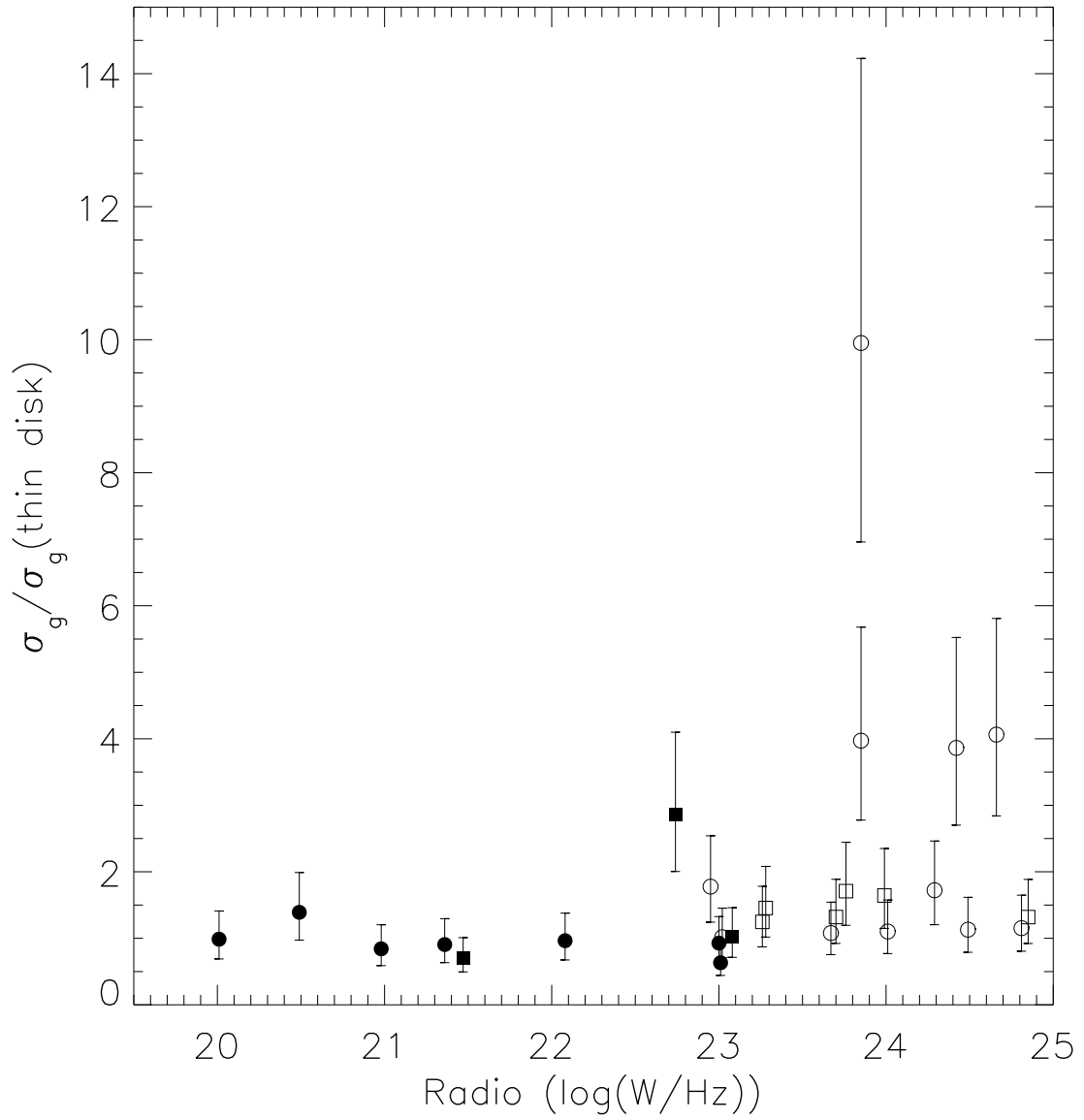


Fig. 7. | R_{ord} versus total radio power at 1.4 GHz for radio galaxies (open symbols) and non-radio galaxies (filled symbols). As shown before, radio galaxies have systematically larger R_{disk} . However, no systematic trend is seen between the radiative power of the AGN at radio wavelengths and the excess dispersion within the radio galaxy sample.

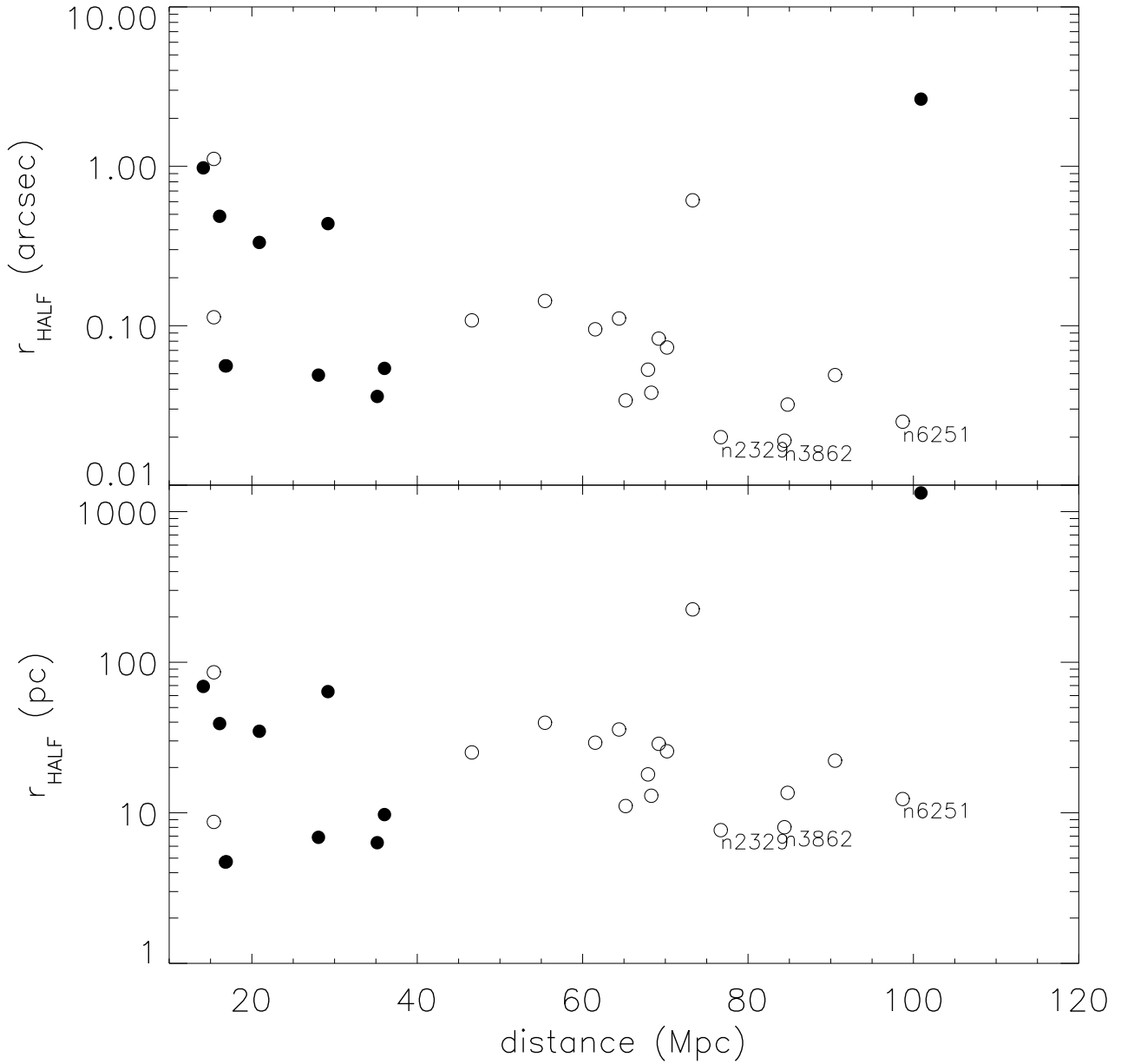


Fig. 8. | Top : angular radius inside which half of the total gas emission is contained versus distance for radio galaxies (open circles) and non-radio galaxies (filled circles). The half light radius of the PSF for these observations is $0.05^{\prime\prime}$. Bottom : same as top panel, but now the half light radius is expressed in parsec.

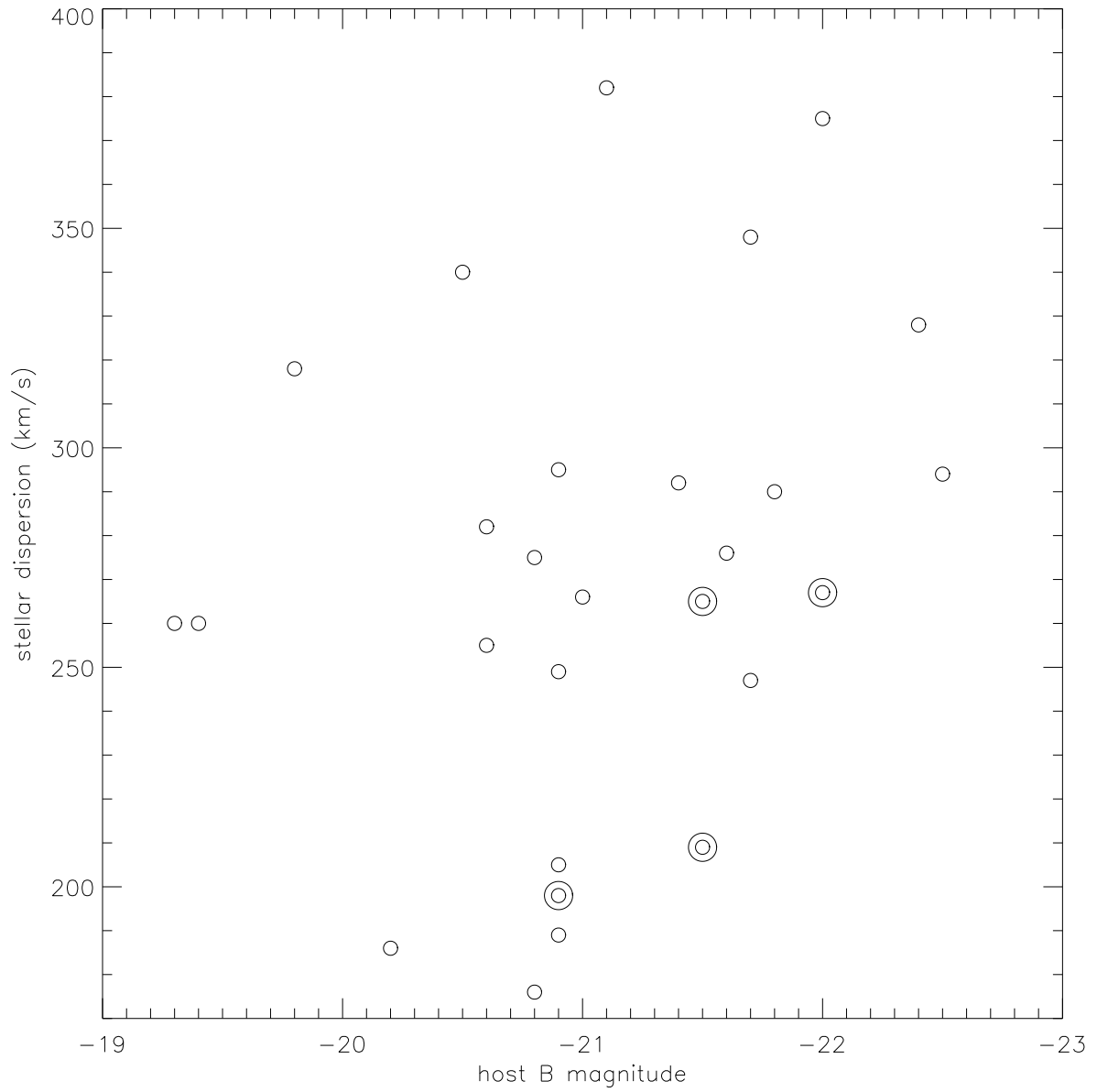


Fig. 9. | Stellar velocity dispersion as a function of host magnitude for the sample galaxies. Galaxies with dust disks with $i < 40$ are indicated by a double circle.

Table 1. Early-Type Galaxy Sample

Galaxy	Type	FRI	D (M pc)	M _B (mag)	s (km /s)	g (km /s)	M (10 ⁸ M _⊙)	L _{radio} log(W /Hz)	ref
(1)	(2)	(3)	(4)	(5)	(6)	(7)	(8)	(9)	(10)
IC 989	E		101	-20.8	176	174 :	...	22.74	r3
IC 1459	E		29	-20.5	340 ^b	532	1.3	23.00	b1,r4
NGC 315	E	1	68	-22.4	328	528 ²	...	24.01	r1
NGC 383	E/SO	1	65	-22.0	267	924 ²	...	24.42	r1
NGC 541	E/SO	1	73	-21.5	209	336	...	23.85	r1
NGC 741	E	1	70	-22.5	294	424	...	23.76	r1
NGC 2329	E/SO	1	77	-21.7	247	301	...	23.67	r1
NGC 3078	E		35	-20.9	249	262	...	23.01	r5
NGC 3245	SO		21	-20.0	205 ^b	168 ¹	2.1	20.49	b2, r6
NGC 3862	E	1	84	-21.5	265	302	...	24.66	r1
NGC 3998	SO		14	-19.8	318	650 ¹	...	21.47	r7
NGC 4278	E		16	-19.3	260	372 ¹	...	22.08	r6
NGC 4335	E	1	62	-20.6	282 ^c	248 ²	< 1.0	23.02	b3,r1
NGC 4374	E	1	15	-20.9	295	883	3.6	23.26	b4,r1
NGC 4459	SO		17	-20.2	186 ^b	193	0.7	20.01	r3
NGC 4486	E	1	15	-22.0	375 ^b	681 ²	29.0	24.81	b6,r1
NGC 4526	SO		36	-19.4	260	424	...	21.36	r3
NGC 5077	E		36	-20.8	275	417	...	23.08	r5
NGC 5127	E	1	64	-20.9	189	157	...	23.99	r1
NGC 5490	E	1	69	-21.4	292	280 ²	...	23.70	r1
NGC 6251	E	1	99	-21.8	290 ^b	434 ¹ :	7.8	24.49	b7,r7
NGC 6861	E/SO		28	-21.1	382 ^d	814	...	20.98	r8
NGC 7052	E	1	55	-21.0	266 ^b	456	3.1	22.95	b8,r1
NGC 7626	E	1	47	-21.6	276	349 ²	...	23.28	r1
UGC 1841	E	1	85	-21.7	348	592 ²	...	24.85	r1
UGC 7115	E	1	91	-20.9	198	545:	...	23.85	r1
UGC 12064	E/SO	1	68	-20.6	255	496 ²	...	24.29	r1

Note. | General properties of the galaxy sample. Col.(2): Hubble classification from the LEDA catalogue (<http://leda.univ-lyon1.fr/>). Col.(3): galaxies indicated by a 1 contain large scale Fanaro & Riley type 1 (1974) radio-jets. Col.(4): distances from Faber et al. (1989), Tonry et al. (2001), or, if not available, directly from observed recession velocity and $H_0 = 75 \text{ km s}^{-1} \text{ Mpc}^{-1}$. Col.(5): Absolute blue magnitude from LEDA. Col.(6): central stellar velocity dispersions typically integrated over an aperture area of several arcsec². The dispersions are from the LEDA catalogue except for: ^b: Tremaine et al. (2002); ^c: Verdoes Kleijn et al. (2002); ^d: from Koprolin & Zeilinger (2000). See Section 2 for discussion of the errors. Col.(7): gas velocity dispersions of narrow H + [N II] and [S III] emission-lines as measured from HST spectra at the

central aperture. See Section 2 for discussion of the errors. These measurements are taken from the literature or obtained by us (indicated by \ast). A 1 indicates that a broad H γ line was fitted in addition to the narrow-lines of the H γ + [N II] complex. A 2 indicates that a broad H γ line is perhaps present (cf. Section 6). A "!" indicates galaxies for which a larger dispersion is measured just outside the central aperture (see Section 2 for details). Col.(8): black hole masses from detailed dynamical gas disk modeling reported in the literature. Col.(9): total radio luminosities at 1.4 GHz (assuming a spectral index $\alpha = 0.75$ for $f_\nu \propto \nu^{-\alpha}$). Col.(11): BH mass references: b1: Cappellari et al. (2002); b2: Barth et al. (2001); b3: Verdoes Kleijn et al. (2002); b4: Bower et al. (1998); b5: Sarzi et al. (2001); b6: Macchetto et al. (1997); b7: Ferrarese & Ford (1999); b8: van der Marel & van den Bosch (1998). Radio emission references: r1: Condon & Boderick (1988); r3: Dressel & Condon (1978); r4: Wright & Otrupcek (1990); r5: Griith et al. (1994); r6: Becker, White & Helfand (1995); r7: White & Becker (1992); r8: Mauer et al. (2003).

Table 2. Spectroscopic properties and results

Galaxy	program	ap		R_1	R_2	$I_1=I_2$	i	ref
(1)	(2)	$(\theta)^2$		(θ)	(θ)	(6)	()	(8)
IC 989	7354	0.1	0.05	$3.3 \cdot 10^2$	$1.6 \cdot 10^0$	$2.2 \cdot 10^1$	60 ^a	
IC 1459	7352	0.1	0.05	$9.0 \cdot 10^3$	$2.7 \cdot 10^1$	$3.6 \cdot 10^2$	60	1
NGC 315	8236	0.1	0.05	$1.7 \cdot 10^2$	$2.0 \cdot 10^1$	$4.7 \cdot 10^3$	77	5
NGC 383	8236	0.1	0.05	$2.0 \cdot 10^2$	$2.1 \cdot 10^2$	$3.8 \cdot 10^2$	40	5
NGC 541	8236	0.2	0.1	$1.4 \cdot 10^2$	$5.3 \cdot 10^1$	$1.9 \cdot 10^3$	25	5
NGC 741	8236	0.2	0.1	$4.3 \cdot 10^2$	$4.4 \cdot 10^3$	$4.4 \cdot 10^2$	60 ^a	5
NGC 2329	8236	0.2	0.1	$1.2 \cdot 10^2$	$8.9 \cdot 10^3$	$3.2 \cdot 10^2$	47	5
NGC 3078	9163	0.2	0.1	$2.0 \cdot 10^2$	$3.2 \cdot 10^1$	$4.0 \cdot 10^4$	63	
NGC 3245	7403	0.2	0.05	$2.0 \cdot 10^1$	$6.4 \cdot 10^2$	$1.6 \cdot 10^1$	63	2
NGC 3862	8236	0.2	0.1	$1.1 \cdot 10^2$	$2.0 \cdot 10^4$	$3.7 \cdot 10^2$	08	5
NGC 3998	7354	0.1	0.05	$1.6 \cdot 10^2$	$6.2 \cdot 10^1$	$8.2 \cdot 10^3$	60 ^a	
NGC 4278	7403	0.2	0.05	$2.6 \cdot 10^2$	$3.8 \cdot 10^1$	$1.7 \cdot 10^2$	42	
NGC 4335	8236	0.2	0.1	$5.7 \cdot 10^2$	$5.8 \cdot 10^2$	$4.4 \cdot 10^2$	66	5
NGC 4374	7124	0.2	0.05	$2.1 \cdot 10^2$	$7.3 \cdot 10^1$	$8.7 \cdot 10^3$	60 ^a	5
NGC 4459	7361	0.2	0.25	$2.2 \cdot 10^2$	$9.2 \cdot 10^2$	$3.4 \cdot 10^2$	47	3
NGC 4486	8666	0.2	0.05	$6.7 \cdot 10^2$	$2.2 \cdot 10^3$	$4.6 \cdot 10^2$	52	5
NGC 4526	9163	0.2	0.05	$3.3 \cdot 10^2$	$1.1 \cdot 10^2$	$3.6 \cdot 10^2$	80	
NGC 5077	7354	0.1	0.05	$3.2 \cdot 10^2$	$3.1 \cdot 10^2$	$3.9 \cdot 10^2$	60 ^a	
NGC 5127	8236	0.2	0.1	$6.4 \cdot 10^2$	$9.4 \cdot 10^2$	$5.3 \cdot 10^2$	60 ^a	5
NGC 5490	8236	0.2	0.1	$5.0 \cdot 10^2$	$1.4 \cdot 10^3$	$4.2 \cdot 10^2$	60 ^a	5
NGC 6251	6653	0.1	0.1	$1.0 \cdot 10^2$	$4.1 \cdot 10^2$	$3.1 \cdot 10^2$	32	4
NGC 6861	9163	0.2	0.1	$2.9 \cdot 10^2$	$1.0 \cdot 10^4$	$3.8 \cdot 10^2$	74	
NGC 7052	8236	0.1	0.05	$2.3 \cdot 10^2$	$1.7 \cdot 10^1$	$2.9 \cdot 10^2$	73	5
NGC 7626	8236	0.2	0.1	$2.3 \cdot 10^2$	$7.3 \cdot 10^2$	$7.0 \cdot 10^1$	60 ^a	5
UGC 1841	8236	0.2	0.1	$1.9 \cdot 10^2$	$1.5 \cdot 10^2$	$4.0 \cdot 10^2$	60 ^a	5
UGC 7115	8236	0.2	0.1	$1.8 \cdot 10^2$	$7.0 \cdot 10^2$	$4.8 \cdot 10^2$	18	5
UGC 12064	8236	0.1	0.05	$2.3 \cdot 10^2$	$2.6 \cdot 10^3$	$3.9 \cdot 10^2$	57	5

Note. | Col.(2): HST program number of spectral observations. Col.(3): size of central aperture through which θ_g was measured. The spectra are obtained using the HST/STIS spectrograph with the G750M grating except for IC 1459 for which the G430L grating was used and NGC 6251 for which the HST/FOS spectrograph with the G780H grating was used. Col.(4)–(6): parameters R_1 , R_2 and $I_2=I_1$ of the unconvolved

emission-line surface brightness profile $I(R) = I_1 \exp(-R/R_1) + I_2 \exp(-R/R_2)$ fitted to the observations. Col.(7): inclination used in disk modeling. The inclination has been determined by us or other authors from larger scale dust disks present in sources except those indicated with a ^a. For these sources an $i = 60^\circ$ was assumed (see Section 2 for details). Col.(9): references for the galaxies for which we used flux measurements (and gas velocity dispersions) reported in the literature. 1: Cappellari et al. (2002); 2: Barth et al. (2001); 3: Sarzi et al. (2001); 4: Ferrarese & Ford (1999); 5: Noel-Storr et al. (2003).